ACS APPLIED MATERIALS & INTERFACES

www.acsami.org

Research Article

Thermoresponsive Liposomes for Photo-Triggered Release of Hypericin Cyclodextrin Inclusion Complex for Efficient Antimicrobial Photodynamic Therapy

Alice Abu Dayyih,[§] Bernd Gutberlet,[§] Eduard Preis, Konrad H. Engelhardt, Muhammad Umair Amin, Ahmed M. Abdelsalam, Martina Bonsu, and Udo Bakowsky*

Cite This: *ACS Appl. Mater. Interfaces* 2022, 14, 31525−31540

Read Online

ACCESS | Metrics & More | Article Recommendations | Supporting Information

ABSTRACT: Antimicrobial strategies with high efficacy against bacterial infections are urgently needed. The development of effective therapies to control bacterial infections is still a challenge. Herein, near-infrared (NIR)-activated thermosensitive liposomes (TSL) were loaded with the NIR-dye 1,1-dioctadecyl-3,3,3,3-tetramethylindotricarbocyanine iodide (DiR) and the water-soluble hypericin (Hyp) β-cyclodextrin inclusion complex (Hyp-βCD). DiR and Hyp-βCD loaded thermosensitive liposomes (DHβCD-TSL) are functionalized for photothermal triggered release and synergistic photodynamic therapy to eliminate the gram-positive *Staphylococcus saprophyticus*. The dually active liposomes allow the production of heat and singlet oxygen species with the help of DiR and Hyp, respectively. The elevated temperature, generated by the NIR irradiation, irreversibly damages the bacterial membrane, increases the permeation, and melts the liposomes via a phase-transition mechanism, which allows the release of the Hyp-βCD complex. The photodynamic effect of Hyp-βCD eradicates the bacterial cells owing to its toxic oxygen species production. DHβCD-TSL measured the size of 130 nm with an adequate encapsulation efficiency of 81.3% of Hyp-βCD. They exhibited a phase transition temperature of 42.3 °C, while they remained stable at 37 °C, and 44% of Hyp-βCD was released after NIR irradiation (T > 47 °C). The bacterial viability dropped significantly after the synergistic treatment (>4 $\log_{10}$), indicating that the NIR-activated TSL have immense therapeutic potential to enhance the antibacterial efficacy. The liposomes showed good biocompatibility, which was confirmed by the cellular viability of mouse fibroblasts (L929).

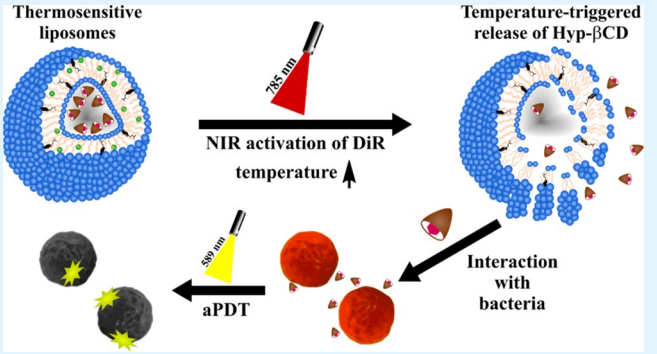

KEYWORDS: *thermosensitive liposomes, triggered release, hypericin, cyclodextrin inclusion complex, antimicrobial, antibacterial, photodynamic therapy, photothermal therapy, near-infrared activated liposomes*

1. INTRODUCTION

One primary goal of modern clinical microbiology is to develop efficient strategies to treat infections caused by microbial pathogens. In 2014, the World Health Organization (WHO) issued a report stating that the "post-antibiotic era" is rapidly approaching, "in which common infections and minor injuries can kill".[1] It was reported that the number of deaths related to global antibiotic resistance will increase to 10 million per year by 2050.[2] Therefore, there is an urgent need to utilize alternative treatment methods against antibiotic-resistant bacteria. In this regard, a promising approach is antimicrobial photodynamic therapy (aPDT). A review published in Lancet Infectious Diseases summarized the alternatives for using antibiotics, including antibodies, enzymes, bacteriophages, and peptides, only to name a few.[3] Oddly, aPDT was not mentioned in this comprehensive review as an approach to fight antibiotic-resistant microbes.[4] More and more research has been conducted on aPDT efficacy against microbial infections in the last few years. A wide variety of photosensitizers was used to eradicate bacterial infections, for example, porphyrin to eliminate methicillin-resistant *Staphylococcus aureus* (MRSA),[5] radochlorin to eradicate MRSA and *E. coli*,[6] hypericin against planktonic and biofilm-forming *Staphylococcus aureus*,[7] and toluidine blue O to eliminate pan drug-resistant strains of *A. baumannii*.[8] Recently, aPDT was proposed and even used to help mitigate the impact of the

Received: February 14, 2022
Accepted: May 30, 2022
Published: July 5, 2022

coronavirus disease 2019 (COVID-19) pandemic either by preventing infections or treating infected patients.[9−11]

aPDT is based on three individual factors: a photosensitizer (PS), light, and molecular oxygen. After irradiation with light of a specific wavelength, the PS can either transfer energy or an electron to molecular oxygen resulting in the formation of singlet oxygen (type II reaction) or reactive oxygen species (ROS) (type I reaction), which can ultimately lead to cell death. Dual selectivity is one of the most significant advantages of aPDT over conventional antibiotic therapy. To begin with, cells with fast growth rates, like bacteria, accumulate PS selectively, and, to a lesser extent, the photodestructive effect is limited to the area to which light is directed.[12] Hypericin (Hyp), a potent nontoxic PS, found in *Hypericum perforatum* L. (St John's Wort), has been reported in aPDT showing good antibacterial abilities.[13] In light of its high singlet oxygen quantum yield ($\Phi_\Delta{}^1O_2$ = 0.29−0.44, in various carriers or solutions) and its cytoplasmic membrane localization nature, it is not surprising that Hyp-mediated aPDT could effectively inhibit Gram-positive bacteria.[14,15] This includes *Staphylococcus saprophyticus* subsp. *bovis*,[16] methicillin-sensitive, and methicillin-resistant *Staphylococcus aureus*,[13] *Streptococcus mutants*,[17] and *Propionibacterium acnes*.[18] However, the clinical applications of Hyp are hampered because of its high hydrophobicity, which in turn hinders its direct application in the biological milieu. Moreover, enhancing the water solubility of Hyp could be a promising approach to improve its bioavailability. In this regard, Hyp can be solubilized with *β*-cyclodextrin polymer (*β*CD). The water-soluble *β*CD polymer is well known to selectively form inclusion complexes, where its feature to solubilize pharmaceutics was widely exploited in the literature.[19,20]

Recently, nanotechnology-based antibacterial approaches have been reported for their enhanced efficacy and therapeutic index.[21] Stimuli-responsive smart nanoparticles, which can respond to diverse exogenous or endogenous stimuli, e.g., pH change, enzymatic degradation, light response, or elevated temperature, are used to enhance the delivery of various drugs.[22] In particular, thermosensitive liposomes (TSL) with tuned release were generally used in the clinic to deliver drugs to the target site.[23] Typically, liposomes consist of a lipid bilayer that undergoes a temperature-dependent phase transition between gel and liquid phases, enhancing the membrane permeability, which allows rapid release of the entrapped drug.[24,25] In this regard, near-infrared (NIR) irradiation can be exploited to increase the temperature above the phase transition temperature through a photothermal reaction making TSL suitable for controlled drug release. Additionally, NIR irradiation can reach deeper tissue parts with minimal damage to the surrounding tissue. It can also disrupt the permeability and denature the proteins of the pathogenic cell wall, ultimately causing bacterial cell death.[26,27]

Combining photothermal therapy (PTT) with aPDT has been an effective synergistic therapy.[28] Unlike PTT, aPDT is conditional on the PS capability to produce ROS, which can destroy the element components of the bacteria like lipids and proteins, leading to their death. Additionally, it is assumed that the elevated temperature from the PTT enhanced the permeability of the bacterial cell wall, which facilitates the uptake of the PS, therefore enhancing the aPDT efficiency.[29] Moreover, diverse polymeric or inorganic nanoparticles have been exploited for their inherent photothermal capacity.[25,29,30] 1,1-Dioctadecyl-3,3,3,3-tetramethylindotricarbocyanine (DiR) iodide is an NIR fluorescent dye with high fluorescence intensity that can be utilized to introduce photothermal capabilities to the carrier in which it is encapsulated.[31] Unlike inorganic or polymeric nanomaterials, DiR has a better degradability and negligible cytotoxicity at concentrations suitable for in vivo imaging and PTT applications.[32,33] Being highly hydrophobic,[34] DiR would be ideal for being encapsulated in the bilayer of TSL, where it allows NIR facilitated disruption of the liposomal membrane, ultimately releasing its cargo.

In this study, the near-infrared dye (DiR) and the hypericin *β*-cyclodextrin complex (Hyp-*β*CD) were encapsulated in thermosensitive liposomes (DH*β*CD-TSL) by thin-film hydration and dehydration−rehydration vesicle (DRV) methods (Figure 1). The dually active thermosensitive liposomes are capable of the photo-triggered release of Hyp-*β*CD and their photoactivation to eradicate bacteria. Physical properties of the Hyp-*β*CD complex, e.g., phase solubility, photostability, and degradation, were investigated. The physical characteristics of liposomes, e.g., size, zeta potential, morphology, and photothermal response, were exploited. The antimicrobial photodynamic activity was performed against gram-positive bacteria, where the capabilities of the near-infrared triggered release of Hyp-*β*CD were assessed. All in all, the properties of the proposed smart system indicate excellent potential for application in antimicrobial therapy. They could be used to treat local infections, e.g., on the skin, gums, or mucous membranes, to minimize commonly occurring systemic side effects of antibiotic treatment.

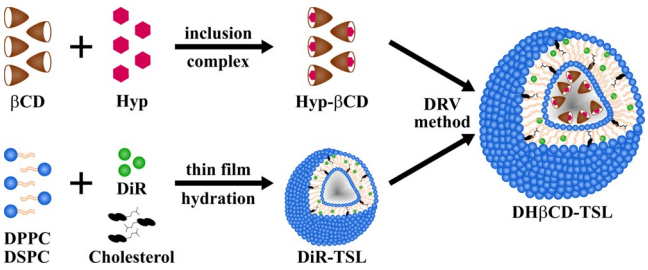

Figure 1. Graphical illustration of hypericin *β*-cyclodextrin inclusion complex (Hyp-*β*CD), DiR thermosensitive liposomes (DiR-TSL), and DiR and Hyp-*β*CD loaded thermosensitive liposomes (DH*β*CD-TSL) preparation methods.

2. MATERIALS AND METHODS

2.1. Materials. Hypericin (Hyp) and 1,3-diphenyl isobenzofuran (DPBF) were purchased from Thermo Fisher Scientific GmbH (Karlsruhe, Germany). DiR (1,1-dioctadecyl-3,3,3,3-tetramethylindotricarbocyanine, iodide) was obtained from Santa Cruz Biotechnology Inc. (Heidelberg, Germany). 2-Hydroxypropyl-*β*-cyclodextrin (*β*CD), cholesterol, 3-[4,5-dimethylthiazol-2-yl]-2,5-diphenyltetrazolium bromide (MTT), fluorescein diacetate (FDA), and propidium iodide (PI) were purchased from Sigma Aldrich Chemie GmbH (Taufkirchen, Germany). 1,2-dipalmitoyl-*sn*-glycero-3-phosphocholine (DPPC), and 1,2-distearoyl-*sn*-glycero-3-phosphocholine (DSPC) were gifted by Lipoid GmbH (Ludwigshafen, Germany). Sodium dodecyl sulfate (SDS) was obtained from Sigma Aldrich (Darmstadt, Germany). Ultrapure water was used for all the experiments. It was generated by PURELAB flex 4 equipped with a point-of-use biofilter (ELGA LabWater, High Wycombe, UK).

2.2. Bacterial Strains and Media. Glycerol stock cultures of *Staphylococcus saprophyticus* subsp. *bovis* (*S. saprophyticus*, DSM 18669, DSMZ, Braunschweig, Germany) were prepared and stored

https://doi.org/10.1021/acsami.2c02741
ACS Appl. Mater. Interfaces 2022, 14, 31525−31540

at −80 °C. The stocks were thawed and cultured in a Mueller Hinton broth (MHB, Sigma Aldrich Chemie GmbH) using an orbital shaker (Compact Shaker KS 15 A, equipped with Incubator Hood TH 15, Edmund Bühler GmbH, Bodelshausen, Germany) set at 200 rpm and 37 °C.

2.3. Cell Culture Conditions. Mouse fibroblast cell line (L929) was purchased from DSMZ. The cells were cultivated in Dulbecco's Modified Eagle Medium (DMEM) from Capricon Scientific (Ebsdorfergrund, Germany) at 37 °C and 5% CO_2 under humid conditions. The media were supplemented with 10% fetal calf serum (PAA, Cölbe, Germany).

2.4. Light Source. The irradiation experiments presented in this work were performed with a Weberneedle Endo Laser (Weber medical GmbH, Lauenförde, Germany),[35] which was equipped with two laser modules depending on the irradiated dye, i.e., Hyp or DiR. The first laser module (λ = 785 nm, 500 mW) was intended for DiR, and the second laser module (λ = 589 nm, 50 mW) for Hyp. Both laser modules were equipped with an optical fiber to convey the laser beam from the Weberneedle Endo Laser to the samples. By adjusting the distance between the irradiated surface and the optical fiber, the diameter of the irradiated spot could be fixed to the size of a single well of a multi-well plate.

In the experiment concerning the photodynamic efficiency (Section 2.9.8), a custom-made LED device (Lumundus GmbH, Eisenach, Germany) was used. The dominant wavelength was at 587 nm, and by adjusting the current to 20 mA, an irradiance of 1.2 mW/cm^2 was obtained.

2.5. Preparation of DiR-TSL and Empty Liposomes. Empty and DiR liposomes were prepared using the thin-film hydration method. Empty liposomes and DiR thermosensitive liposomes (DiR-TSL) were prepared by dissolving DPPC (T_m = 41 °C), DSPC (T_m = 55 °C), cholesterol, and DiR (in case of DiR-TSL) in a molar ratio of (70:25:5) and (70:22:5:3), respectively, in chloroform:methanol (2:1) v/v. The organic solvents of the lipid and lipid/drug mixture were evaporated under an escalating vacuum using the rotary evaporator Heidolph Laborota 4000 efficient (Heidolph Instruments, Schwabach, Germany). The resulting lipid film was hydrated with 10 mM HEPES buffer (pH 7.4) to obtain a final concentration of 10 mg/mL of liposomes. The crude vesicles were formed using an ultrasound bath sonicator (Bandelin Sonorex RK 100H, Bandelin Electronic, Berlin, Germany) for 30 min at 60 °C. Liposomes were stored in the dark at 4 °C for further use.

2.6. Production of Hypericin-β-Cyclodextrin Complex (Hyp-βCD). The formation of the hypericin β-cyclodextrin (Hyp-βCD) inclusion complex was performed according to a method previously described.[12] Briefly, Hyp dissolved in methanol was dried under a rotary evaporator (Heidolph Laborota 4000, Heidolph Instruments, Schwabach, Germany) until a thin Hyp film was formed. Furthermore, a 5% βCD in ultrapure water solution was added to the Hyp film followed by 15 min of sonication. The obtained mixture was then left to stir for 24 h. The complex was withdrawn and centrifuged at 20,000 rcf (Mikro 220, Andreas Hettich GmbH, Tuttlingen, Germany) for 10 min to remove any unsolubilized Hyp. The amount of Hyp in the complex was then determined by UV−vis (UV Mini 1240, Shimadzu Corp., Japan) according to the calibration curve of Hyp in methanol:5% βCD (1:1) v/v. A clear red solution was obtained, which was stored at 4 °C for further use.

2.7. Production of Dehydration−Rehydration Vesicles (DRVs). Hyp-βCD were encapsulated into empty (Hyp-βCD-TSL) and DiR-TSL (DHβCD-TSL) by the DRV method.[36] Liposomes that were previously produced by the thin-film hydration method according to Section 2.5 were mixed with Hyp-βCD produced in Section 2.6 in a ratio of 4:1 v/v, resulting in a final concentration of 198 μM of Hyp-βCD. The physical mixture was then shaken for 15 min followed by rapid freezing using liquid nitrogen. Afterward, the samples were freeze-dried (Christ Alpha 1−4 LSC, Martin Christ, Germany). The finished lyophilized mixture was hydrated with 200 μL of warm ultrapure water and incubated in a water bath for 30 min at 60 °C. Then, subsequent hydration with 800 μL of warm 10 mM HEPES buffer followed by further incubation for 30 min at 60 °C. The free Hyp-βCD complex was separated from the prepared liposomes using size exclusion chromatography (SEC) (Sephadex-G25 column, PD-10 Columns, GE Healthcare, Germany). Prepared liposomes were kept in the dark at 4 °C until further use.

2.8. Characterization of Hyp-βCD Complex. *2.8.1. Phase Solubility Study.* Phase solubility studies of Hyp in an aqueous solution of βCD were conducted according to the method reported by Higuchi and Connors.[37] Briefly, aqueous concentrations (ranging from 0.648−32.446 mM) of βCD, equivalent to (0.1−5%) (w/v), of βCD in 1:1 of 10 mM HEPES buffer and ultrapure water were first prepared. After adding an excessive amount of Hyp to each of the βCD solutions, the acquired mixtures were stirred at 25 °C for 48 h. Aliquots were withdrawn and centrifuged for 15 min (Mikro 220, Andreas Hettich GmbH, Tuttlingen, Germany). The absorbance of the supernatant was measured at λ = 590 nm by a UV-photometer (UV Mini 1240, Shimadzu Corp., Japan) to determine the amount of Hyp, according to the calibration curve of Hyp in methanol:5% βCD (1:1) v/v. The diagram of phase solubility was obtained by plotting the concentration of Hyp against the concentration of βCD. Moreover, UV-spectra of the Hyp-βCD complex with the same amounts of βCD used in the solubility study were also acquired.

2.8.2. ^{1}H-NMR Spectroscopy. The formation of the Hyp-2-hydroxypropyl-β-cyclodextrin (Hyp-βCD) complex had to be confirmed before it could be incorporated into liposomes. For this purpose, we investigated the complexation between hypericin and 2-hydroxypropyl-β-cyclodextrin (βCD) using ^{1}H NMR spectroscopy (nuclear magnetic resonance spectroscopy). Free hypericin, βCD powder, and the lyophilized Hyp-βCD were dissolved in 0.5 mL of DMSO-D_6 or D_2O and were measured using an ECZ400S NMR spectrometer (JEOL GmbH, Freising, Germany).[38] The spectra were processed using MestReNova 6.1.0 (Mastrelab).

2.8.3. Photostability of Free Hypericin and Hypericin β-Cyclodextrin Inclusion Complex. The photostability of Hyp in both MeOH and β-cyclodextrin inclusion complex was analyzed during the irradiation. A total of 200 μL of each sample was pipetted onto a 96-well plate with a final Hyp concentration of 40 μM. Samples were irradiated with diode laser module yellow (λ = 589 nm, 50 mW, 100% power intensity) for 0, 5, 10, 15, 20, 25, and 30 min, and the absorbance spectrum was recorded for each time spectrophotometrically.

2.9. Characterization of Liposomes. *2.9.1. Size and Zeta Potential.* Hydrodynamic diameters of the liposomes were measured after diluting in ultrapure water (1:100) using dynamic light scattering (DLS) (Zetasizer Nano ZS, Malvern Panalytical, Herrenberg, Germany), which is equipped with a 10 mW HeNe laser at the wavelength of 633 nm. The scattered light was detected at an angle of 173°. The zeta potential values were determined using laser doppler velocimetry (LDV).[39] The obtained results were presented as the average value ± standard deviation of three independent preparations with three replicate measurements of each formulation for at least 10 runs.

2.9.2. DiR and Hyp-βCD Entrapment Efficiency and Drug Loading. Free DiR and free Hyp-βCD were separated from liposomes by size exclusion chromatography using the Sephadex G25 column. The column was saturated beforehand with empty liposomes followed by the addition of loaded liposomes. The eluted liposomes were diluted 1:10 with methanol. The encapsulation efficiency was determined spectrophotometrically (λ_{Hyp} = 590 nm, λ_{DiR} = 785 nm) according to precalculated calibration curves using a Multiskan GO UV/Vis microplate spectrophotometer (Thermo Fisher Scientific GmbH, Germany).[12] The encapsulation efficiency was determined using the following eq 1:

$$\mathrm{EE\%} = \frac{\text{entrapped amount of drug}}{\text{initial amount of drug}} \times 100\% \quad (1)$$

Drug loading capacity (DLC %) was calculated as the amount of drug entrapped in liposomes versus the total drug and initial amount of the drug and the lipid added during formulation according to the following eq 2:

https://doi.org/10.1021/acsami.2c02741
ACS Appl. Mater. Interfaces 2022, 14, 31525−31540

$$\text{DLC\%} = \frac{\text{amount of entrapped drug}}{(\text{initial amount of drug} + \text{intial amount of lipids})} \times 100\% \quad (2)$$

2.9.3. Atomic Force Microscopy (AFM). The morphology of the DHβCD-TSL was investigated using the atomic force microscope (AFM), NanoWizard 3 NanoScience AFM (JPK BioAFM Business, Bruker Nano GmbH, Berlin, Germany). The morphology of DHβCD-TSL was assessed before and after NIR irradiation (λ = 785 nm, 500 mW) for 30 min. Briefly, 20 μL of DHβCD-TSL was diluted in ultrapure water (1:100) and then pipetted onto a silicon wafer. DHβCD-TSL were left for 5 min for sedimentation, and the excess liquid was aspirated, leaving a thin film of aligned vesicles on the wafer. The cantilevers were of type HQ:NSC14 Al/BS with a length of 125 μm, a resonance frequency of 140 kHz, and a force constant of 5 N/m. All measurements were done in AC mode. The images were acquired with a size of 1 × 1 μm at a scan speed of 1.5 Hz.[40]

2.9.4. Transmission Electron Microscopy (TEM). The morphological integrity of DHβCD-TSL was also investigated using the transmission electron microscope (TEM) JEM-3010 (JEOL) with a retractable high-resolution slow-scan CCD-Camera (Gatan MegaScan 794). The morphology of DHβCD-TSL was assessed before and after NIR irradiation (λ = 785 nm, 500 mW) for 30 min, where liposomes were subjected to TEM visualization at 80 kV. Liposomes were diluted 1:100 with 10 mM HEPES buffer (pH 7.4) before staining with uranyl acetate (2%) for 30 min. Liposomes were pipetted onto 300 mesh formvar coated S160−3 copper grids (Plano GmbH, Wetzlar, Germany). Equal parts of the sample and uranyl acetate were mixed, and the grid was incubated for 5 min in this solution. The mixture was examined at an accelerating voltage of 300 kV and 110 μA emission current with current densities between 50 and 60 pA/cm^2.

2.9.5. Differential Scanning Calorimetry (DSC). The phase transition temperature of lyophilized DHβCD-TSL, DiR-TSL, and empty-TSL was measured using DSC-7 Perkin Elmer (Rodgau, Germany). Additionally, the influence of increasing mole fractions of DiR in relation to the lipid was assessed (1, 3, 5, 7, and 10% (mol/mol)). The reference cells were filled with an empty disk, and the baseline was subtracted from the thermogram of liposomes. DSC scans were analyzed using Pyris software, and the peak maximum was set as the transition temperature (T_m).

2.9.6. Photothermal Characterization of Liposomes. A total of 100 μL of liposomes was pipetted onto a 48-well plate and irradiated for 30 min with NIR irradiation (λ = 785 nm, 500 mW, 60% power intensity) with a final DiR concentration of 65 μM. The temperatures and photographs of the NIR-irradiated liposome solutions were recorded at designated intervals (0, 5, 10, 15, 20, 25, and 30 min). Single wells were irradiated, and the temperature change was analyzed at several time intervals by thermal imaging (FLIR ONE Pro, FLIR Systems, Inc., Wilsonville, OR, USA).

2.9.7. Light Triggered Release of Hyp-βCD from Liposomes. A total of 1 mL of DHβCD-TSL (325 μM of DiR and 198 μM of Hyp-βCD) was pipetted onto a 48-well plate (NUNC, Thermo Fischer Scientific GmbH, Germany). NIR irradiation (λ = 785 nm, 500 mW, 60% power intensity) was applied for 10, 20, and 30 min. The liposomes were transferred to a 6 mL glass vial, and the liposomes were allowed to free release in 4 mL of 10 mM HEPES buffer (pH 7.4). The vials were placed at 37 °C and 200 rpm on a thermostatically controlled magnetic stirrer (IKA-Werke, Staufen, Germany). At selected time intervals (0.25, 0.5, 1, 2, and 4 h), a 500 μL release medium was retrieved and centrifuged at 23,000 rcf (Mikro 220, Andreas Hettich GmbH, Tuttlingen, Germany). The absorbance of the supernatant was measured at λ = 590 nm by a UV-photometer (UV Mini 1240, Shimadzu Corp.) to determine the amount of the released Hyp-βCD according to the calibration curve of Hyp in methanol:5% βCD (1:1) (v/v). The cumulative release was defined using the following eq 3:

$$\text{cumulative release\%} = \frac{\text{amount of released Hyp} - \beta\text{CD}}{\text{amount of loaded Hyp} - \beta\text{CD in liposomes}} \times 100\% \quad (3)$$

2.9.8. Photodynamic Efficiency of DHβCD-TSL in Solution. Photodynamic activity of hypericin either in the free complexed (Hyp-βCD) or the liposomal formulation was qualitatively evaluated using 1,3 diphenyl isobenzofuran (DPBF) as a singlet molecular oxygen quencher.[41] A total of 10 mg of the DPBF was dissolved in 10 mL of 0.1 M sodium dodecyl sulfate under sonication to attain the maximum solubility of the dye. The solution was then filtered using a 0.2 μm syringe filter. Hypericin formulated as βCD-complex or in the TSL before and after NIR treatment was diluted using the DPBF solution so that the final hypericin concertation reached 1.1 × 10^{-7} M. Samples were further transferred to a 96-well plate suitable for UV measurements (Nunc, Thermo Fisher, Germany). The well plate was irradiated using a yellow LED at 20 mA and 1.2 mW/cm^2 at several time intervals (0, 5, 10, 15, 20, 25, 30, 35, and 40 s). Changes in the UV-absorption spectra of DBPF resulting from consecutive irradiation were recorded using a Multiskan GO UV/vis microplate spectrophotometer. The hypericin complex and TSL liposomes were employed as blanks. The quantum yields of the free Hyp-βCD and the DHβCD-TSL were calculated using the quantum yield of rose bengal as a known reference using the following equation:

$$\Phi_\Delta^S = \frac{k_S}{k_R} \times \Phi_\Delta^R \times \frac{F^R}{F^S}$$

where k_S and k_R are the degradation rate constants for the sample and reference PS, respectively. The Φ_Δ^R is the quantum yield of rose bengal as the reference PS. F is the absorption correction factor given by $F = 1-10^{-\text{OD}}$ (OD is the optical density at the irradiation wavelength).[42]

2.10. Bacterial Viability Assay. For the determination of antimicrobial activity, the liposomes were incubated with bacterial suspensions and irradiated. The growth of the bacterial suspension was stopped by placing it on ice at an optical density (OD_{600}) of 0.4, measured with a spectrophotometer (Shimadzu UV mini-1240, Kyoto, Japan). A total of 100 μL of this suspension was incubated with an equal volume of the liposomes (final concentration 40 μM Hyp or/and 65 μM of DiR) under light protection for 30 min at room temperature and 100 rpm using an orbital shaker (Compact Shaker KS 15 A, equipped with Incubator Hood TH 15, Edmund Bühler GmbH, Bodelshausen, Germany). A total of 100 μL of this solution was pipetted into a 48-well plate (TC plate, Standard, F, Sarstedt AG & Co. KG) and irradiated with NIR (λ = 785 nm, 500 mW, 60% power intensity) and either with or without yellow-laser (λ = 589 nm, 50 mW, 100% power intensity) for 30 min, respectively. After irradiation, the suspensions were serially diluted with MHB and plated onto Mueller Hinton II Agar plates (BD, Heidelberg, Germany). After incubating the plates for 18 h at 37 °C and 90% relative humidity, the viable colonies were counted, and the colony-forming units per milliliter were calculated (CFU/mL). DHβCD-TSL, DiR-TSL, and Hyp-βCD-TSL were compared to empty thermosensitive liposomes and dark control groups without irradiation. The experiments were performed in triplicates under light-protected conditions.

2.11. CLSM Bacterial Viability Measurements. A bacterial suspension was prepared as described above (Section 2.2), and the bacteria have adhered to a round coverslip. After a washing step with sterile phosphate-buffered saline (PBS), the coverslips were covered with 100 μL of DHβCD-TSL in the same concentration as in the bacterial viability assay and irradiated for the same time (Section 2.10). In the meantime, an FDA and a PI stock solution have been prepared. These were added to sterile PBS to make the staining solution (FDA 8 μg/mL, PI 20 μg/mL). After the irradiation, the coverslips were washed with PBS and incubated in the staining solution for 5 min to visualize the live and dead bacteria of the various samples. After a further washing step, the samples were analyzed with a Zeiss LSM700 confocal laser scanning microscope (Carl Zeiss Microscopy GmbH, Jena, Germany).

https://doi.org/10.1021/acsami.2c02741
ACS Appl. Mater. Interfaces 2022, 14, 31525−31540

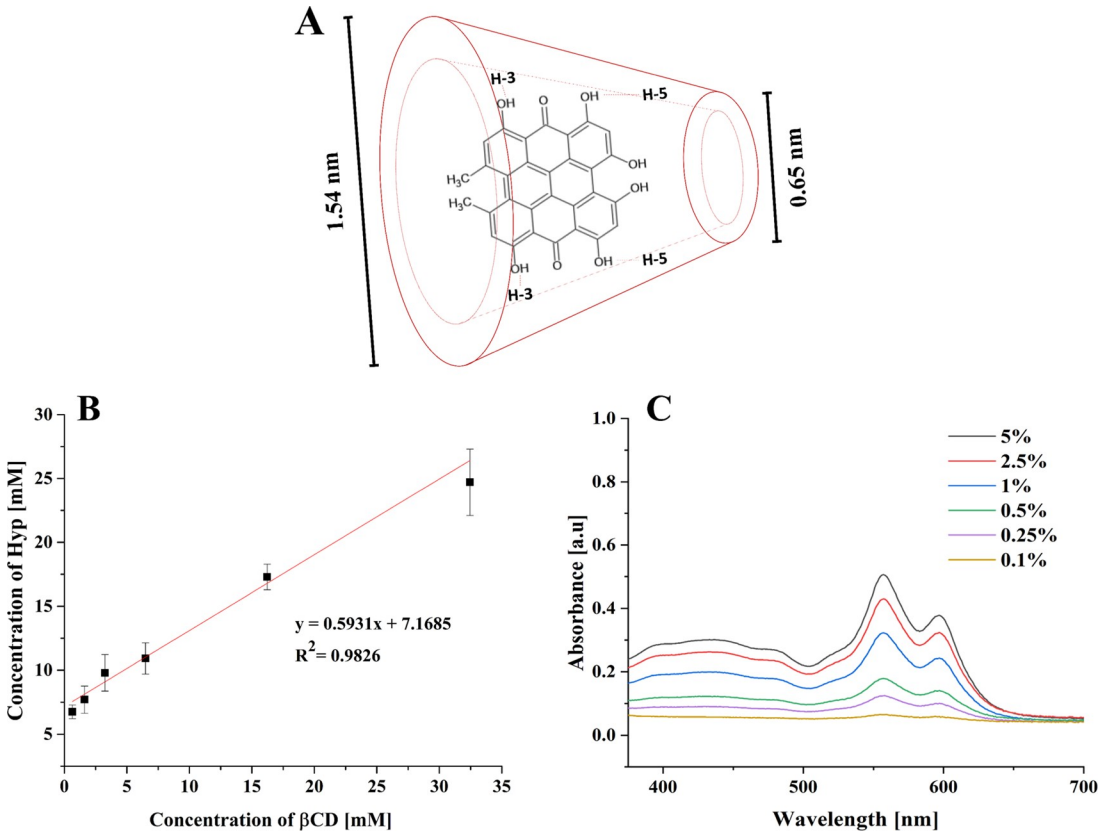

Figure 2. (A) Schematic representation of a possible hypericin β-cyclodextrin inclusion mode.[46] (B) Phase solubility diagram of the hypericin β-cyclodextrin complex system at 37 °C. (C) UV−vis spectra of hypericin β-cyclodextrin with different concentrations of β-cyclodextrin % (w/v) in aqueous solution (pH 7.4, 25 °C) (n = 3).

2.12. Cellular Biocompatibility. Cytotoxicity of the empty and loaded liposomes and free Hyp-βCD complex was determined by the MTT assay against L929 cells. Cells were seeded at a density of 25,000 cells/well onto a 48-well plate (NUNC, Thermo Fischer Scientific GmbH, Germany) and incubated for 24 h until full adherence. A total of 200 μL of liposomes/medium combination with a final concentration of 40 μM of HβCD, βCD, or/and 65 μM of DiR was placed in each well and was incubated for 24 h in the dark. Then, the medium was aspirated, and MTT reagent 1:10 was added to each well. Afterward, the cells were incubated for 4 h in the dark. During this time, viable cells convert the water-soluble MTT to water-insoluble purple formazan crystals, which can be solubilized in DMSO and quantified by measuring the absorption at 570 nm using a plate reader (FLUOstar, BMG, Germany). The values of cells incubated with medium represent 100% viability, and TritonX was used as a positive control.

2.13. Statistical Analysis. All experiments were performed in triplicates, and the results are presented as mean ± standard deviation (SD) unless explicitly stated otherwise. A two-tailed t-test was performed to determine significance, and probability values of $p < 0.05$ were considered significant. Statistical differences are denoted as "*" $p < 0.05$, "**" $p < 0.01$, "***" $p < 0.001$, and "****" $p < 0.0001$.

3. RESULTS AND DISCUSSION

3.1. Synthesis and Characterization of Hyp-βCD Complex. The application of hypericin (Hyp) in the biological milieu is rather limited because of its high hydrophobicity. To improve the water solubility of Hyp, we used β-cyclodextrin (βCD) as a solubilizing agent. We studied the formation of a water-soluble inclusion complex between Hyp and βCD; there was no chemical synthesis involved to preserve the original structure of Hyp. In addition to being convenient and efficient, the method would provide a highly water-soluble Hyp with high water solubility and bioavailability.[19] A series of studies were conducted to evaluate the efficiency of the inclusion complex formation.

3.1.1. Phase Solubility Study. Phase solubility studies are useful for studying the inclusion complexation of hydrophobic compounds with cyclodextrin molecules (Figure 2A) in an aqueous solution. Stepwise addition of βCD to ultrapure water led to a linear increase in the concentration of Hyp, as shown in Figure 2B. The slope value of the linear plot was 0.5931, with a correlation coefficient of 0.983. A stoichiometry of 1:1 between the complex and the Hyp system can be considered the A_L type (linear diagram), following Higuchi and Connors.[37] Moreover, UV−vis spectra of Hyp-βCD with different concentrations of βCD were acquired (Figure 2C). Since the βCD solution has no observable peaks in the visible UV region,[43] only the Hyp peaks can be observed at 558 and 597 nm. It was found that the peak positions at 558 and 597 nm were independent of the concentrations of Hyp-βCD. However, the intensity of the peaks becomes greater with an increased concentration of βCD. Our results indicated that βCD as a solubilizer improved the aqueous solubility of Hyp, forming an inclusion complex of Hyp, which may invade the βCD cavities thanks to hydrophobic interactions. Additionally, complexation efficacy with cyclodextrins usually is low; therefore, a higher concentration of cyclodextrins is used in the industry.[20] Moreover, in a series of studies in our lab, 5% of βCD was considered optimum.[12,44,45] To that end, and following the phase solubility study results, 5% of βCD was used to form the Hyp-βCD inclusion complex.

https://doi.org/10.1021/acsami.2c02741
ACS Appl. Mater. Interfaces 2022, 14, 31525−31540

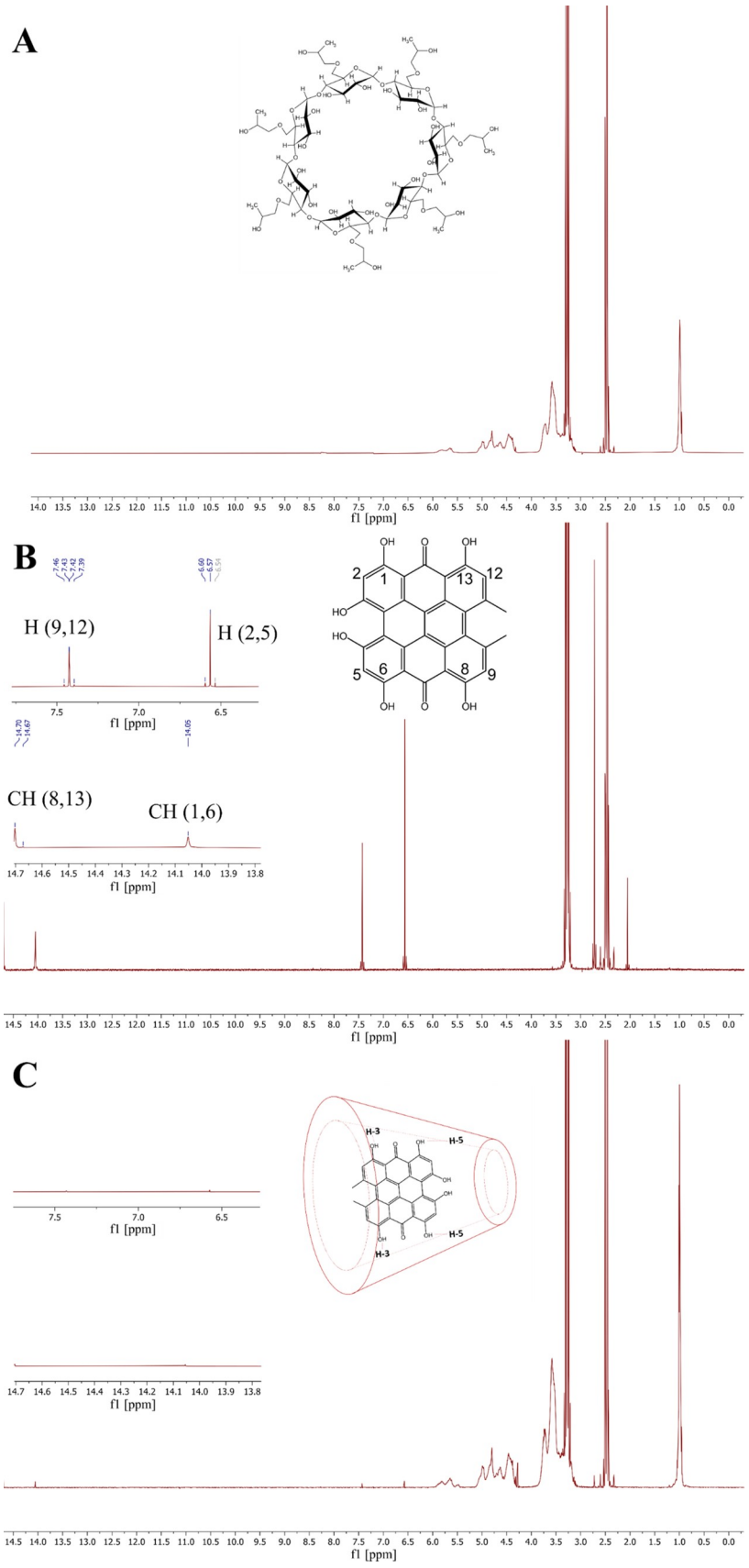

Figure 3. ^{1}H NMR spectra of (A) β-cyclodextrin in DMSO-D_2O, (B) hypericin in DMSO-D_2O, and (C) hypericin β-cyclodextrin inclusion complex in D_2O.

https://doi.org/10.1021/acsami.2c02741
ACS Appl. Mater. Interfaces 2022, 14, 31525−31540

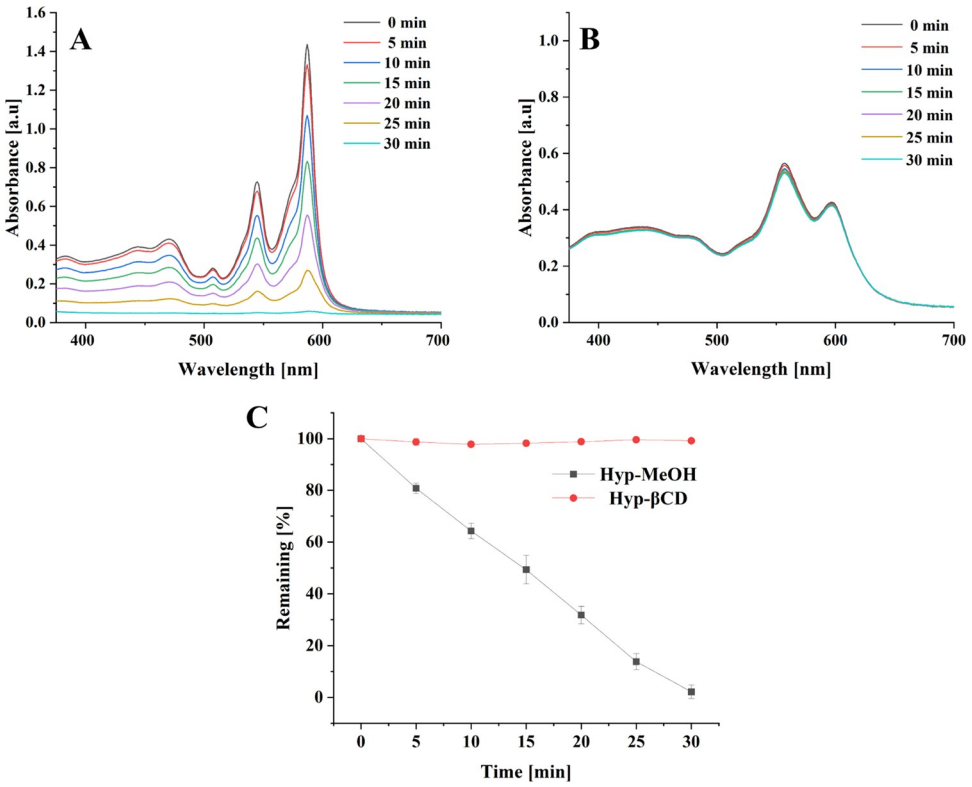

Figure 4. UV−vis spectra of (A) free hypericin in MeOH. (B) Hypericin β-cyclodextrin in an aqueous medium (pH 7.0, 25 °C) irradiated for 30 min using a Weberneedle laser (λ = 589 nm, 50 mW, 100% power intensity). (C) Summary of both (A) and (B) highlighting the remaining absorption at 587 nm (n = 3).

Table 1. Characterization of Liposomes[a]

liposomes	size ± SD [nm]	PdI ± SD	ZP ± SD [mV]	EE ± SD [%]	DLC ± SD [%]
empty	93.3 ± 6.6	0.26 ± 0.04	−3.8 ± 1.5		
Hyp-βCD-TSL	120.6 ± 2.1	0.19 ± 0.02	−21.4 ± 2.0	87.2 ± 4.3 (Hyp-βCD)	0.86 ± 0.05 (Hyp-βCD)
DiR-TSL	84.6 ± 8.3	0.19 ± 0.03	18.9 ± 4.9	85.7 ± 1.5 (DiR)	2.5 ± 0.1 (DiR)
DHβCD-TSL	133.5 ± 16.6	0.20 ± 0.03	−15.8 ± 6.3	72.4 ± 3.2 (DiR) 81.3 ± 4.1 (Hyp-βCD)	2.1 ± 0.2 (DiR) 0.80 ± 0.04 (Hyp-βCD)

[a]Hydrodynamic diameter (size), polydispersity index (PdI), zeta potential (ZP), encapsulation efficiency (EE %), and drug loading capacity (DLC %). The hydrodynamic diameter is expressed as a measure of particle size distribution by intensity (mean ± SD, n = 3).

3.1.2. ^{1}H-NMR Spectroscopy. The direct evidence of the formation of the Hyp-βCD inclusion complex could be found in the ^{1}H NMR spectrum.[38,47] The efficiency of the Hyp-βCD complexation was studied by comparing the ^{1}H NMR spectra of Hyp in the absence and presence of βCD (Figure 3B,C, respectively). The chemical structure of βCD can be shown in Figure 3A. The ^{1}H NMR spectrum of βCD corresponds well with the previously reported spectrum.[19] The typical Hyp ^{1}H NMR spectrum is shown in Figure 3B, consistent with the previous report.[48] Moreover, Figure 3C confirms the formation of the Hyp-βCD complex, since the intensity signals of protons of the aromatic region (OH(1), OH(6), OH(8), and OH(13)) decreased significantly, agreeing with the results acquired in multiple studies.[19,20,49] Our results indicate that Hyp monomers have invaded the β-cyclodextrin cavities forming an inclusion complex. The inclusion complex is formed via hydrophobic interactions mediated by supramolecular interactions.

3.1.3. Photostability of Free Hypericin and Hypericin β-Cyclodextrin Inclusion Complex. The photobleaching phenomenon refers to the decrease of absorbance and/or fluorescence of the photosensitizer upon illumination.[50] The photosensitizer must not deteriorate too quickly to affect the infection site positively. However, controlled photodegradation aims to eliminate the remaining photosensitizer after the treatment to limit patients' photosensitivity following aPDT treatment.[51] Figure 4 displays photodegradation of free Hyp dissolved in MeOH and Hyp in the β-cyclodextrin inclusion complex irradiated using Weberneedle module (λ = 589 nm, 50 mW, 100% power intensity) as a function of time. Free Hyp showed a continuous decrease in the bands 554 and 587 nm. Hyp photodegradation in the cyclodextrin inclusion complex was significantly slower than in the free form. A host−guest structure can attenuate hydrolysis or photolysis of drugs by protecting them from reactive substances.[52] This shielding effect may lead to lower availability and interaction of complexed Hyp molecules with the light source. Barras et al. examined the photodegradation of Hyp in lipid nanocapsules and compared it to free Hyp in DMSO. They have found that the encapsulated Hyp had faster photodegradation than its counterpart.[50] On the contrary, Saw et al. showed that solubilizing Hyp in *N*-methyl pyrrolidine increased its photostability compared to its free counterpart.[53] The slow photodegradation of Hyp in the cyclodextrin inclusion

https://doi.org/10.1021/acsami.2c02741
ACS Appl. Mater. Interfaces 2022, 14, 31525−31540

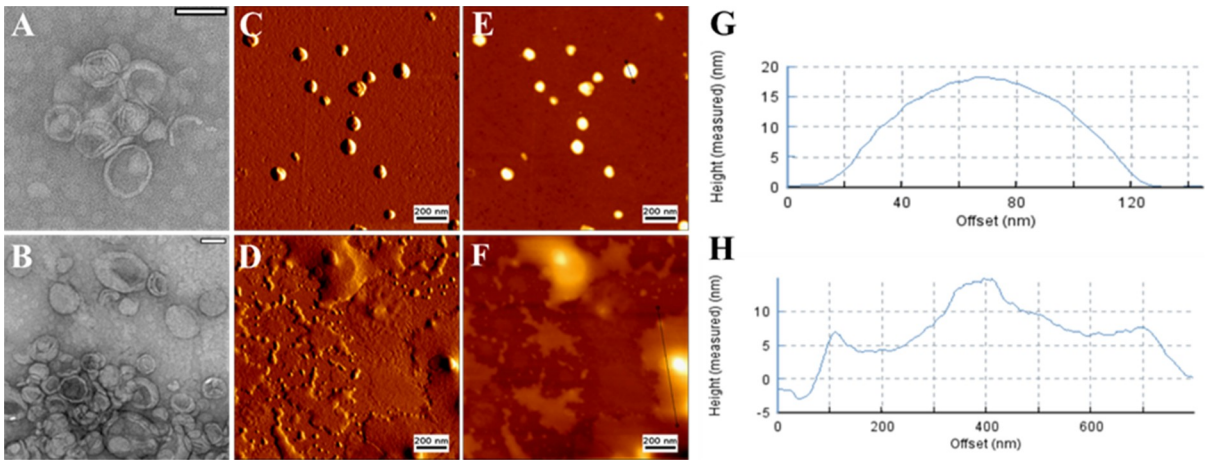

Figure 5. Representative TEM images of (A) DHβCD-TSL at 25 °C and (B) DHβCD-TSL after NIR irradiation (λ = 785 nm, 500 mW). Scale bar: 100 nm. AFM micrographs of (C) DHβCD-TSL at 25 °C and (D) DHβCD-TSL after NIR irradiation (λ = 785 nm, 500 mW). Scale bar: 200 nm. (E, F) Cross sections of liposomes in measured height trace with identified lines. (G, H) Height of the cross-sectional profile along the identified line.

complex is beneficial to assure the delivery of Hyp to the infection site. Thereby, a higher concentration can improve killing efficiency.[54] Cyclodextrins have widely been used as a photoprotective for multiple photosensitive drugs, including quercetin, diclofenac, doxycyclines, sulfanilamide, and retinoids. Incorporating these drugs in cyclodextrin gave rise to a complex characterized by higher drug stability in an aqueous medium and a higher photostability.[55]

3.2. Size and Zeta Potential. The liposomes were fabricated by a classical thin-film hydration method, and the Hyp-βCD complex was loaded through the DRV method.[12] Because of its low solubility, the hydrophobic DiR was encapsulated into the lipid bilayer of the TSL, which makes the lipid shell of the liposomes very susceptible to disruption by NIR irradiation, allowing the escape of Hyp-βCD from the liposomes.[34] The hydrodynamic diameter, polydispersity index, zeta potential, encapsulation efficiency, and drug loading capacity of the liposomes are summarized in Table 1. The average particle size of empty and DiR liposomes was 93.3 ± 6.6 and 84.6 ± 8.3 nm, respectively. Upon the encapsulation of the Hyp-βCD inclusion complex, the size of liposomes increased to 120.6 ± 2.1 and 133.5 ± 16.6 nm, respectively. The increase in the average size could be attributed to the encapsulation of the Hyp-βCD complex. Plenagl et al. observed an increase in the size of the liposomes from 137 to 196 nm upon encapsulation of Hyp-βCD.[12] Liposomes displayed a narrow size distribution with PdI < 0.25 except for the empty liposomes. The DiR encapsulated thermosensitive liposomes (DiR-TSL) showed a positive surface charge of 18.9 ± 4.9 mV, which could be attributed to the positive charge of the DiR dye.[56] The zeta potential changed significantly after the encapsulation of the Hyp-βCD inclusion complex to −15.8 ± 6.3 mV. The decrease in the zeta potential after the encapsulation of Hyp-βCD is attributed to the negative net charge of Hyp because of its vinylogous acid group.[56] The encapsulation efficiencies of DiR and Hyp-βCD in DHβCD-TSL were 72.4 ± 3.2 and 81.3 ± 4.1%, respectively. The encapsulation efficiency of DiR in DiR-TSL was higher than in DHβCD-TSL, achieving 85.7 ± 1.5%. The encapsulation efficiency of Hyp-βCD was high in both Hyp-βCD-TSL and DHβCD-TSL liposomes, which is comparable to previously published data of encapsulating prednisolone-βCD complex in PC/Chol liposomes with an encapsulation efficiency >80%.[57]

3.3. Changes in Morphology. The morphological characteristics of DHβCD-TSL were investigated before and after NIR irradiation using transmission electron microscopy (TEM) and atomic force microscopy (AFM) (Figure 5). The average diameter of DHβCD-TSL before NIR irradiation from both methods corresponded well with the data obtained from DLS measurements (Figure 5A,C). DHβCD-TSL demonstrated well-segregated, homogeneously distributed vesicles below 150 nm.

NIR irradiation led to a significant change in the size of the liposomal vesicles as they appeared to be significantly larger (Figure 5), as demonstrated by TEM images. DLS measurements after NIR irradiation confirmed this change as the liposomes showed a higher diameter, but PdI was not changed significantly (Table S1). Additionally, for AFM, it appeared that the liposomes had undergone a significant morphological change post-irradiation. However, AFM was unable to fully visualize the lipid bilayer meaning that diffused liposomes may appear as a fluidized unit after the deformation of the supported lipid bilayer. We assume that the liposomes have undergone phase changes after the NIR irradiation, and when they were cooling down, liposomes tended to diffuse, forming a giant new unit accompanied by some lipid monolayer formation over the AFM silicon surface.

Moreover, the height image was utilized to assess the disruption of the liposomes. The height of liposomes decreased after NIR irradiation, indicating the destruction of the liposomal integrity. The height of liposomes before NIR irradiation was around 19 nm with a diameter of 120 nm. In contrast, after NIR irradiation, the height of liposomes decreased by about 50% of the original height with a diameter across the diffused liposomal moieties of 800 nm, indicating disruption of the liposomal integrity and diffusion of multiple liposomes after the phase change.

3.4. Thermoresponsive Properties of DHβCD-TSL Liposomes. To evaluate the thermosensitive properties of the liposomes, a series of experiments were conducted before in vitro evaluation. A low power intensity laser was used (785 nm, 500 mW, 60% power) that is suitable to induce a thermal

https://doi.org/10.1021/acsami.2c02741
ACS Appl. Mater. Interfaces 2022, 14, 31525−31540

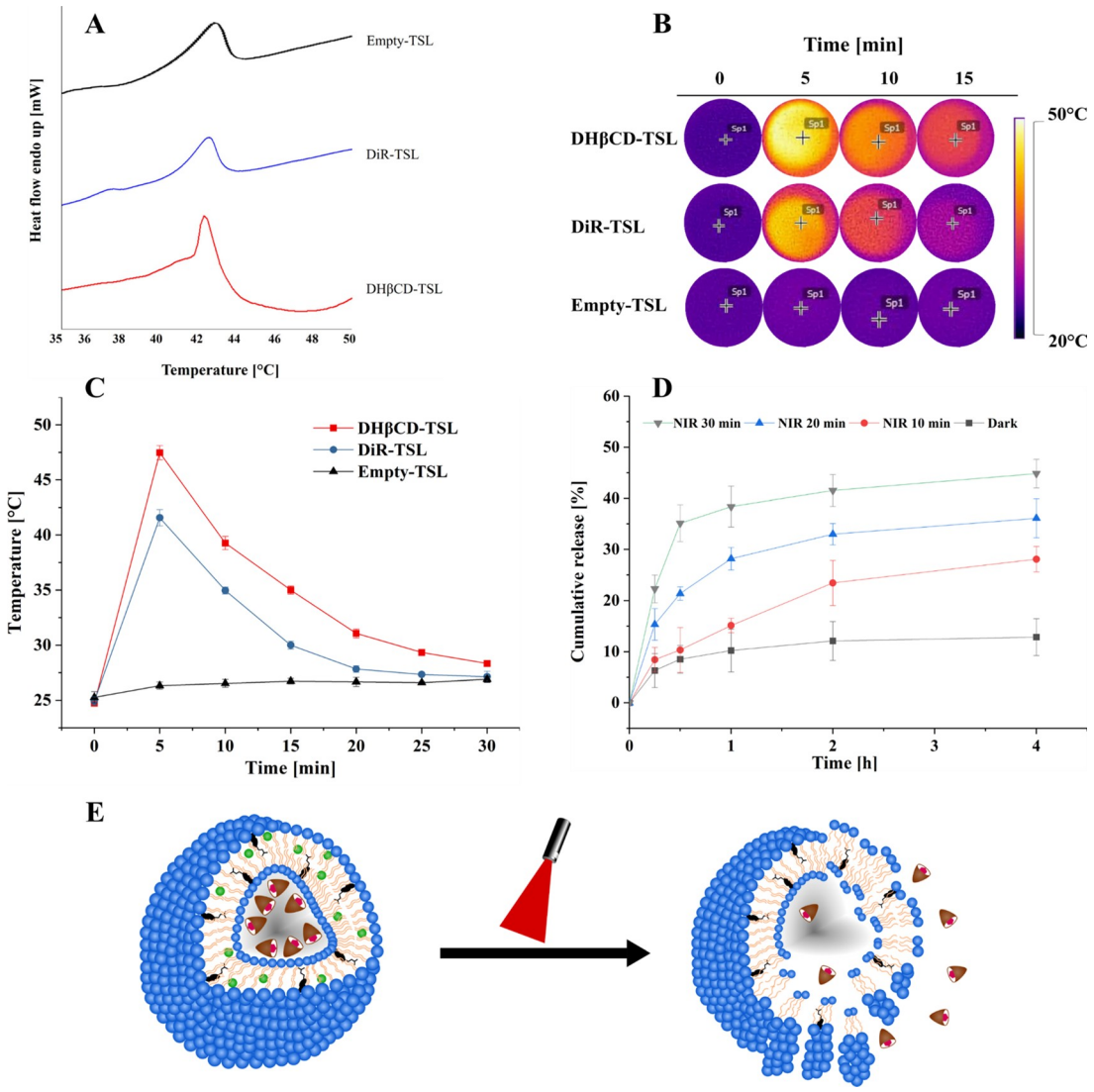

Figure 6. Thermal characterization of liposomes. (A) DSC thermogram of thermosensitive formulations (DHβCD-TSL, DiR-TSL, and empty-TSL) with a scanned temperature range of 30 to 50 °C. The thermograms were adjusted for better visualization. (B) Thermal images of DHβCD-TSL, DiR-TSL, and empty-TSL under NIR irradiation at selected time points. (C) Heating curves of DHβCD-TSL, DiR-TSL, and empty-TSL under NIR irradiation. (D) In vitro cumulative release profile of hypericin β-cyclodextrin from DHβCD-TSL under NIR irradiation at different time points (n = 3). (E) Graphic representation of the TSL during irradiation. For all experiments, NIR irradiation (λ = 785 nm, 500 mW, 60% power intensity) was used.

response in the liposomes and would minimize irreversible damage to ambient healthy tissues.[57]

3.4.1. Differential Scanning Calorimetry (DSC). DSC was employed to determine the temperature required to transform a lipid bilayer from the gel to liquid state. Different lipid ratios in liposomes were prepared, with subsequently recorded DSC thermograms of the obtained liposomes, and a suitable transition temperature was achieved. It was observed that the phase transition temperature of empty liposomes consisting of DPPC:DSPC:cholesterol in a molar ratio of 70:25:5 was around 43.5 °C (Figure 6A), which is a suitable temperature for thermal responsive therapy in a physiological environment.[57] The phase transition temperature (T_m) of DHβCD-TSL exhibited a slight change in the empty liposomes and DiR-TSL (Figure 6A), which was recorded at 42.3 °C. It was noticed that the shift in phase transition temperature depends not only on the subtle blend of the lipid in the formulation but also on the amount of the hydrophobic DiR dye. However, the effect of increasing mole fractions of DiR in relation to lipid on the phase transition temperature (T_m) was minimal (Figure S1). Moreover, in a previous study in our lab, Hyp was found to significantly affect the phase transition temperature of the lipid bilayer in which it is incorporated.[58] We assume that all the Hyp is contained in the aqueous compartment of the liposomes. Moreover, if any small fraction is incorporated in the lipid bilayer, it would probably be a nonsignificant amount to cause any alteration in the phase transition temperature.

3.4.2. Photothermal Activity. The photothermal efficiency of DHβCD-TSL was evaluated by measuring the temperature change during laser irradiation with a thermal infrared camera (Figure 6B,C). When the DHβCD-TSL and DiR-TSL solutions at a concentration of 65 μM DiR were exposed to NIR irradiation for 30 min, the temperature increased in the first 5 min by approximately 22.7 and 16.7 °C, respectively, while no noticeable temperature change was observed of empty liposomes. The elevated temperature was higher in the

https://doi.org/10.1021/acsami.2c02741
ACS Appl. Mater. Interfaces 2022, 14, 31525−31540

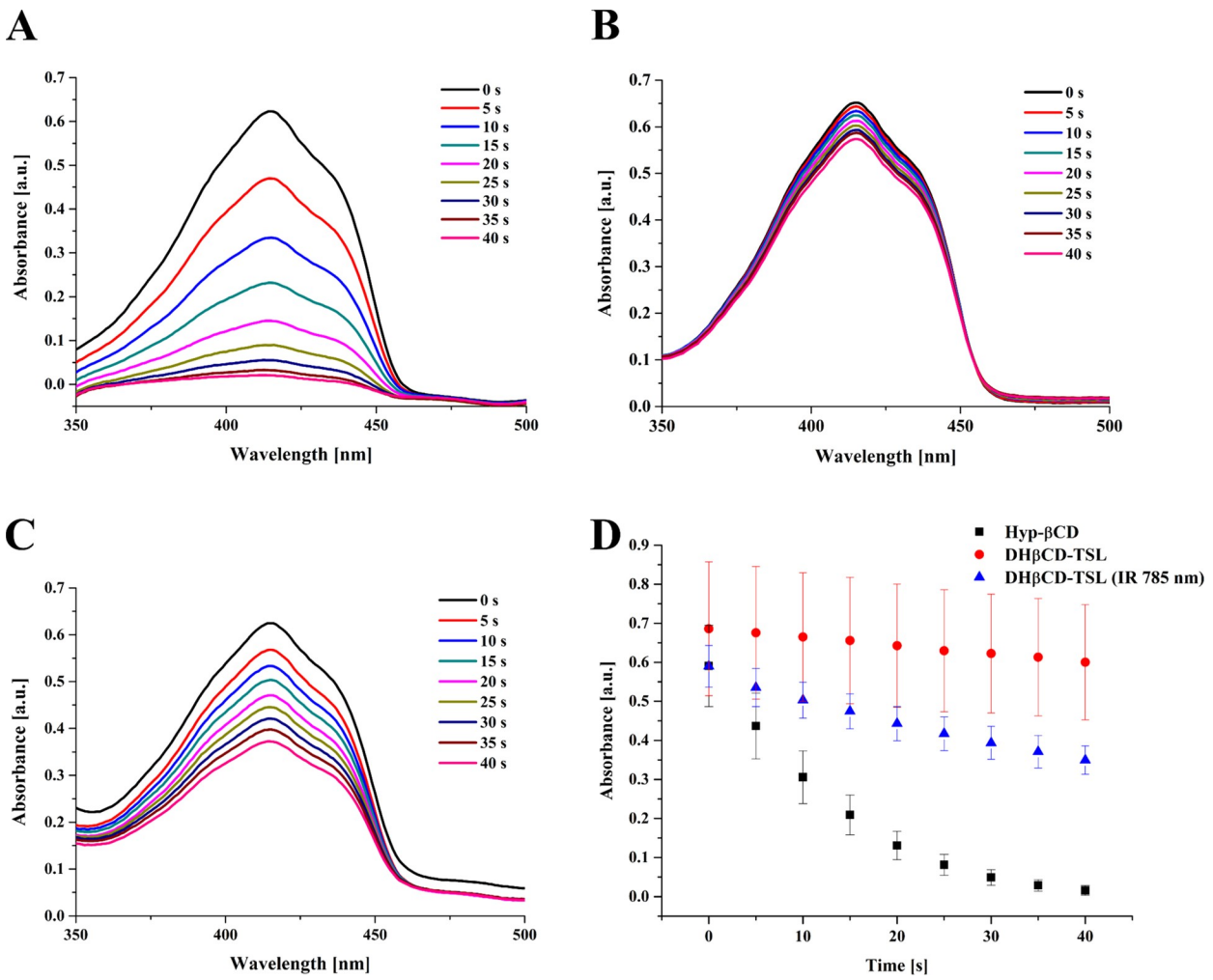

Figure 7. (A) UV/vis absorption curves of DPBF dye comixed with 1.1×10^{-7} M of hypericin β-cyclodextrin complex. (B) TSL and (C) TSL pretreated with NIR (λ = 785 nm, 500 mW, 60% power intensity) for 30 min following consecutive irradiation with yellow LED (587 nm, 1.2 mW/cm^2) for several time intervals. (D) The corresponding reduction in the absorption intensity of DPBF was measured at 415 nm (n = 3).

DHβCD-TSL than in the DiR-TSL solution. In liposomes loaded with both Hyp and DiR, the probability of a small fraction interacting with each other via collisional quenching might be higher, which could be responsible for the higher photothermal performance. The temperature fell exponentially after 5 min, indicating possible photobleaching of DiR. A 22 °C increase could lead to severe irreversible damage to bacterial cell walls if the starting temperature is 37 °C, in vivo or in vitro; therefore, NIR-induced DiR-mediated PTT could be exploited for bacterial eradication.[30]

Moreover, the NIR-laser induced elevated temperature (up to 47.4 °C) is far above the phase transition temperature of DHβCD-TSL liposomes (Figure 6A), which is high enough to activate the thermosensitive liposomes to go through a phase transition, causing the release of the Hyp-βCD complex.

Diverse studies reported the effectiveness of PTT to eradicate or disturb bacterial growth. Preis et al. used indocyanine green (ICG) loaded poly(D,L-lactide) nanofibrous meshes to eliminate *Staphylococcus saprophyticus* subsp. *bovis*, *Escherichia coli* DH5 alpha, and *Staphylococcus aureus* subsp. *aureus* with a combination of PTT (maximum of 54.5 °C) and aPDT.[27] Qing et al. eradicated clinical methicillin-resistant *Staphylococcus aureus* with synergistic antibiotic and IR-780 mediated PTT at a temperature of 49 °C in vivo.[59] Furthermore, on the other extreme, Wang et al. studied the synergistic PTT and aPDT effect of copper-based nanoparticles with temperatures exceeding 90 °C for a short period. They reported successful bacterial eradication of *Staphylococcus aureus* biofilms.[60]

3.4.3. Light Triggered Release. The NIR-responsive Hyp-βCD complex release from DHβCD-TSL was further investigated. In the dark, only a small fraction of Hyp-βCD was released at 37 °C in the duration of 4 h (Figure 6D). NIR-irradiation was applied for 10, 20, or 30 min, where the release measurement started after a total of 30 min for all irradiated samples (Figure 6D). Shortly after 10 min NIR irradiation, the release of Hyp-βCD complex was evident, reaching its maximum of 28.1% after 4 h. By increasing the irradiation time, more and more Hyp-βCD complexes would be released once the NIR irradiation time was increased. For instance, after 30 min of NIR irradiation, the Hyp-βCD complex was released rapidly reaching 35.1% after 0.5 h. Some Hyp-βCD complex continued gradually releasing reaching its maximum of 44.8% after 4 h. According to these results, DiR mediated PTT induced the rapid release of Hyp-βCD from DHβCD-TSL by the photothermal effect generated by NIR exposure. In Figure 6E, a suggested morphological change is shown under NIR irradiation.

https://doi.org/10.1021/acsami.2c02741
ACS Appl. Mater. Interfaces 2022, 14, 31525−31540

3.5. Photodynamic Efficiency of DHβCD-TSL. The development of reactive oxygen species is one prominent feature of PS by which pathogens could be eradicated.[61] The development of reactive species was assessed in solution to predict the behavior of the TSL in further use. DPBF is a famous reactive oxygen quencher that can indirectly assess ROS production via measuring its absorption depletion as a result of increased ROS generation.

In our protocol, we measured the depletion of DPBF as a result of hypericin photoactivation in the complexed and liposomal formulations. The consecutive irradiation of formulations comixed with DPBF at different time intervals is shown in Figure 7. The complexed Hyp-βCD showed drastic degradation in the absorption curve of DBPF as seen in Figure 7A. On the other hand, TSL liposomes showed a weak effect on the DPBF depletion as indicated in Figure 7B. On the contrary, the TSL pretreated with NIR irradiation (785 nm, 500 mW, 60% power intensity) showed a relatively higher depletion effect on the DPBF peaks, as indicated in Figure 7C. Accordingly, the relative depletion in the DPBF absorption measured at 415 nm was primarily high in the Hyp-βCD complex; however, for the TSL liposomes, only the NIR treated candidates showed a notable difference for the DPBF peaks (Figure 7D).

Furthermore, Table 2 shows that the degradation rate of DPBF seems to be linear in all formulations with reasonable regression values. The calculated photodynamic activities were found higher in the case of complexed hypericin as it is in a very soluble form. On the contrary, DHβCD-TSL liposomes showed relatively weaker activity, which might be due to the quenching effect of the complexed hypericin by the DiR dye incorporated in the liposomes. In contrast, the IR-treated liposomes showed higher activity than the non-NIR-treated liposomes.

Table 2. Calculated Degradation Rate Constants of DPBF and Quantum Yields of the Hypericin β-Cyclodextrin Complex, DHβCD-TSL, and DHβCD-NIR Treated TSL in 0.1 M SDS Solution (Mean ± SD, n = 3)

formulations	DPBF depletion constant (k) [sec^{-1}] ± SD	calculated quantum yield (Φ) ± SD	correlation coefficient (r^2) ± SD
Hyp-βCD	0.091 ± 0.020	0.632 ± 0.139	0.989 ± 0.015
DHβCD-TSL	0.003 ± 0.000	0.023 ± 0.001	0.997 ± 0.001
DHβCD-TSL (IR 785 nm)	0.013 ± 0.001	0.089 ± 0.005	0.996 ± 0.001

Irradiation of DHβCD-TSL liposomes with NIR at 785 nm indicated that most of the DiR degraded, and only the peaks corresponding to the Hyp persisted, as shown in Figure 8A. In addition, the linear fit of the normalized DPBF absorption hints at the masking effect of DiR on the generated ROS, indicating a lower depletion rate that tends to be significantly elevated after NIR treatment (Figure 8B). The photodynamic activity of NIR-treated DHβCD-TSL is 3.8 folds higher than non-NIR-treated ones, as indicated in Figure 8C, which can be attributed to the depletion of DiR dye, the destruction of the liposomal architecture, and the release of hypericin.[62]

3.6. Bacterial Viability Assay. Successful antimicrobial photodynamic therapy depends on many factors. Various procedures have already been investigated, but the success depends heavily on the radiation strength and radiant exposure or the overall dosimetry.[63] There are differences for each photosensitizer, and this multifactorial concept in dosimetry should be included in every experiment.[64] The free-form Hyp shows an excellent photodynamic effect but, as already mentioned above, is not suitable for therapy because of its low water solubility and bioavailability.[16] This problem was overcome by using a water-soluble Hyp-βCD complex. The conjugation of a water-insoluble drug to cyclodextrin has already been used to increase the water solubility of some photosensitizers.[65] For example, Hegge et al. tested a cyclodextrin conjugate with curcumin and demonstrated an advantage in terms of thermal stability, photostability, and easier solubilization compared to the ethanolic solution.[66] Cyclodextrins are biocompatible oligosaccharides with a macrocyclic toroidal shape and hydrophobic cavity.[54] According to Ribeiro et al., the affinity of photosensitizers to Gram-negative bacteria is slightly reduced by their conjugation to cyclodextrins, but this is compensated by the improved solubility, availability, and efficiency of the singlet oxygen generation.[67] The selectivity can be improved by incorporating targeting moieties into the complex.[68,69]

In this study, the bacteria were treated with the prepared liposomes and either kept in the dark or irradiated. The results are presented in Figure 9. No dark toxicity of the liposomal formulations could be observed. In addition, the influence of the light source is negligible since no significant changes in viability could be determined when comparing dark and irradiated unloaded liposomes. In contrast, the DHβCD-TSL in the combination of the two wavelengths reduced the bacterial viability significantly by >4.2 $\log_{10}$. Irradiation with a yellow laser alone showed no significant bacterial reduction despite high radiant exposure indicating that the Hyp-βCD complex was completely encapsulated in the liposomes and could only affect the bacterial viability after being released. NIR irradiation alone displayed only a slight reduction in bacterial viability (0.9 $\log_{10}$). Therefore, it can be assumed that most of the antibacterial effect originates from the released Hyp-βCD complex. In contrast, the NIR irradiation of the DiR-TSL showed no reduction, possibly because of the elevated temperature that the liposomes reach when the Hyp-βCD complex is also included. All other formulations exhibited no significant antimicrobial effect. Only the combination of both photosensitizers and both wavelengths showed a bacterial reduction of 99.994% qualifying the formulation as antibacterial, according to the American Society for Microbiology.[44] Our triggerable release formulation was tested on a Gram-positive bacterial strain. Although aPDT generally is limited against Gram-negative bacteria, the antimicrobial effect of Hyp in this regard has already been assessed in recent publications and was proven sufficient.[70,71] The survivability of *Candida albicans* strains as a representative for fungi was similarly reduced by Hyp compared to our results.[72] Additionally, some studies have investigated using aPDT against Coronavirus disease 2019 (COVID-19)[9] and herpes simplex virus.[73]

Because of the excellent efficacy and broad applicability against many different microorganisms, our formulation could be used in many applications of aPDT (e.g., infected wounds on the skin, gum, or mucous membranes). By improving the water solubility and using the controlled release profile of thermosensitive liposomes, our formulation offers the possibility of a physiologically harmless and future-oriented form of application.

https://doi.org/10.1021/acsami.2c02741
ACS Appl. Mater. Interfaces 2022, 14, 31525−31540

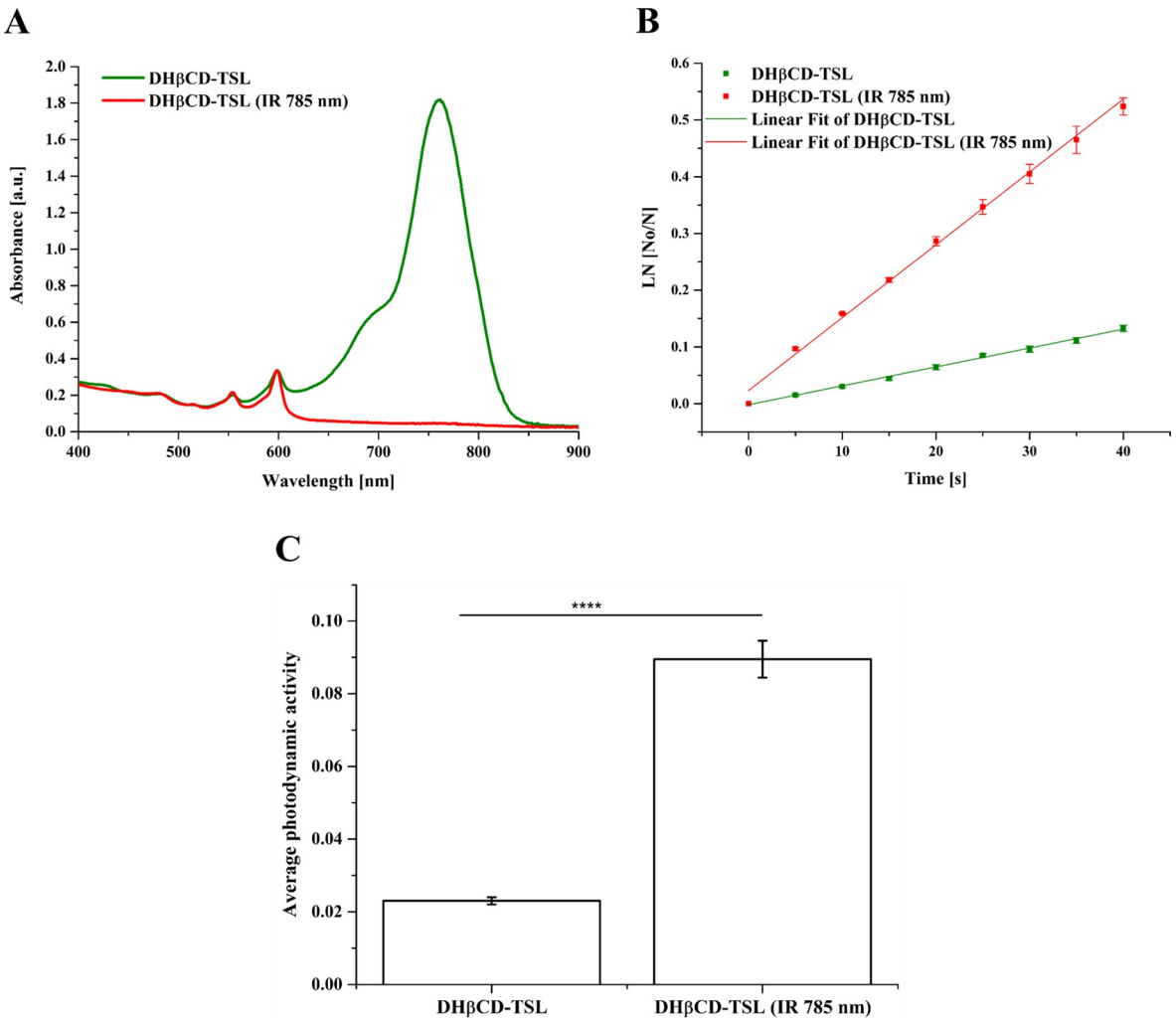

Figure 8. (A) UV/vis absorption curve of DHβCD-TSL liposomes incorporating hypericin β-cyclodextrin and DiR before and after NIR (λ = 785 nm, 500 mW, 60% power intensity) treatment for 30 min. (B) Normalized absorption of DPBF comixed with either DHβCD-TSL or NIR treated DHβCD-TSL for several time intervals and (C) average enhancement of the photodynamic activity of hypericin in DHβCD-TSL after treatment with NIR "****" $p < 0.0001$ ($n = 3$).

3.7. CLSM Bacterial Viability Measurements. The results of the bacteria suspension test were visualized by live/dead staining with FDA and PI and are shown in Figure 10. The non-fluorescent FDA is taken up by living cells and converted into the green fluorescent metabolite fluorescein. Since this only works in living cells, the measured signal is an indicator of viable cells. In contrast, the red pigment PI cannot pass through a viable cell membrane. It only passes through disordered areas of the dead cell membrane and intercalates with the DNA in the cell nucleus, whereby the red color indicates dead cells.[74]

The CLSM images show that the bacteria survived in the presence of DHβCD-TSL without irradiation (Figure 10A). So the DHβCD-TSL alone had no toxic effect on bacteria. Irradiation with a yellow laser also showed no decrease in bacterial survival (Figure 10C), indicating that the Hyp-βCD complex was completely encapsulated in the liposomes and could not have any toxic effects on the bacteria. In the CLSM images of NIR irradiation, you can see a few red dots (Figure 10B) resembling the results of the suspension test, in which there was also a slight reduction in bacterial viability. A reason for this could again be due to the increased temperature after irradiation. Solely the combination of the two wavelengths resulted in an entirely red dotted picture, i.e., dead bacterial cells (Figure 10D). All in all, these CLSM images have successfully visualized and confirmed the bacterial suspension test.

3.8. Cellular Biocompatibility. The cellular biocompatibility of the liposomes and Hyp-βCD were evaluated against L929 cells.[27,75] All formulations showed non to minor toxicity, while free Hyp-βCD showed cellular viability of 85.4% (Figure 11). Thereafter, it was assumed that the utilization of both Hyp-βCD and DiR is safe.

Moreover, it has been reported that β-cyclodextrins demonstrated cellular toxicity if applied continuously for more extended periods. However, the neutral 2-hydroxypropyl-beta-cyclodextrin used in this study has demonstrated lower cytotoxicity in comparison with cationic and anionic β-cyclodextrins.[76] In another study conducted in vivo, intravenous infusion induced some minor clinical observations and biochemical and histopathology changes; however, the application of 2-hydroxypropyl-beta-cyclodextrin was considered safe.[77]

https://doi.org/10.1021/acsami.2c02741
ACS Appl. Mater. Interfaces 2022, 14, 31525−31540

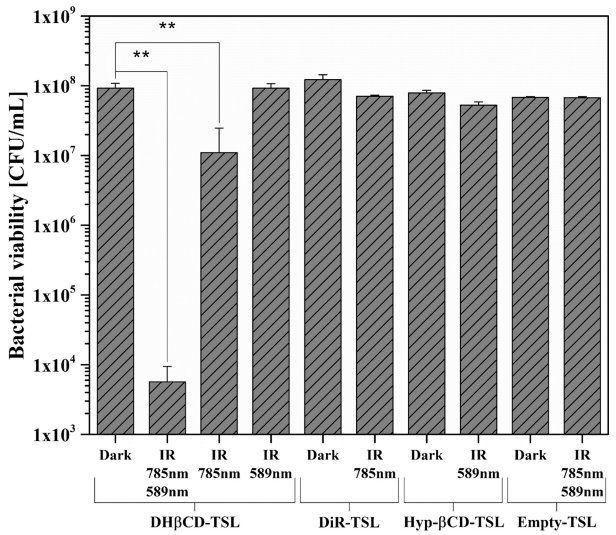

Figure 9. Bacterial viability of *Staphylococcus saprophyticus* subsp. *bovis* (*S. saprophyticus*) after irradiation (IR) with laser modules (NIR: 785 nm, 500 mW, 60% power intensity; yellow-laser: 589 nm, 50 mW, 100% power intensity) and an optical fiber for 30 min each. Empty-TSL was used as the negative control, and dark represents unirradiated bacteria. Probability values of $p < 0.05$ were considered significant. Statistical differences are denoted as "**" $p < 0.01$ ($n = 3$).

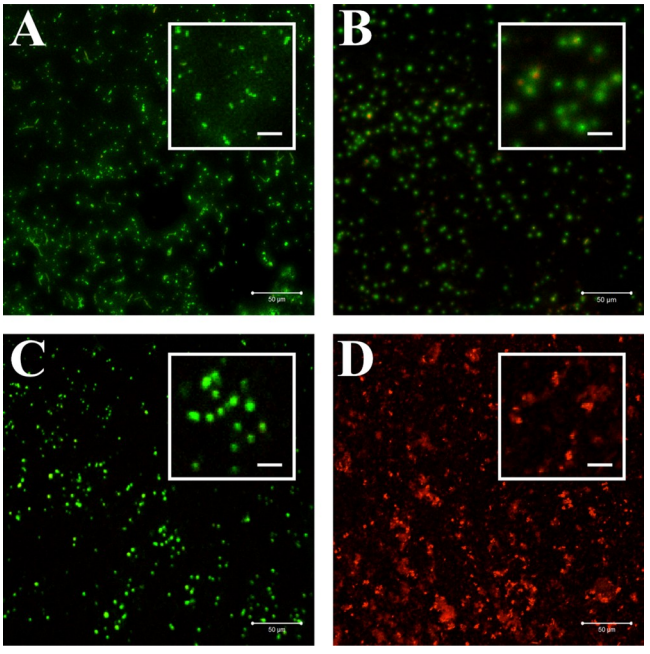

Figure 10. CLSM images of bacteria stained with FDA and PI, which were incubated with DHβCD-TSL in the absence of light (A), incubated with DHβCD-TSL and irradiated with NIR (785 nm, 500 mW, 60% power intensity) (B), yellow laser (589 nm, 50 mW, 100% power intensity) (C), or a combination of the two (D). Scale bars represent 50 and 10 μm for the insets.

4. CONCLUSIONS

The water-soluble host βCD improved the physical properties of Hyp, forming the Hyp-βCD inclusion complex. This work is composed of the characterization of Hyp-βCD, aiming to gain high solubility and stability in water. The subsequently characterized Hyp-βCD was further encapsulated in thermosensitive liposomes to enhance its bioavailability in the infection site. We have designed NIR-activated thermosensitive liposomes for a synergistic antibacterial strategy that incorporates the advantages of triggered drug release via NIR-mediated photothermal therapy and physical damage via photodynamic therapy. The thermosensitive liposomes are homogeneous in size and biocompatible, could maintain their structural integrity at temperatures below 37 °C, and possess controlled thermo-responsive characteristics. In vitro testing demonstrated the controlled release via NIR, where the combined treatments showed a reduction of 4.2 $\log_{10}$ in bacterial viability confirmed by CLSM images. In conclusion, this work provides the feasibility of a new antimicrobial system with a controllable release profile that can kill pathogens and might be beneficial in treating infected wounds on the skin, gum, or mucous membranes.

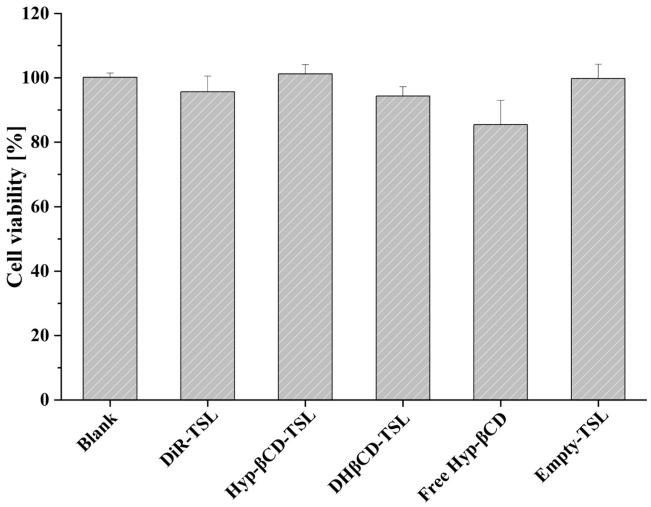

Figure 11. Cellular viability of L929 cells after incubation for 24 h with DiR-TSL, Hyp-βCD-TSL, DHβCD-TSL, free hypericin β-cyclodextrin, and empty liposomes in a final concentration of 40 and 65 μM in terms of hypericin β-cyclodextrin and DiR, respectively. For statistical analysis, the results were compared against blank values ($n = 3$).

■ ASSOCIATED CONTENT

Supporting Information

The Supporting Information is available free of charge at https://pubs.acs.org/doi/10.1021/acsami.2c02741.

Additional experimental data including DSC thermograms of liposomes (DPPC) obtained with the increasing amount of DiR dye (Figure S1) and the characterization of liposomes, i.e., hydrodynamic diameter (size), polydispersity index (PdI), zeta potential (ZP), before and after NIR irradiation (785 nm, 500 mW, 15 min) (Table S1) (PDF)

■ AUTHOR INFORMATION

Corresponding Author

Udo Bakowsky − *Department of Pharmaceutics and Biopharmaceutics, University of Marburg, 35037 Marburg, Germany;* orcid.org/0000-0002-3895-0453; Phone: + 49 (0) 6421 28 25884; Email: ubakowsky@aol.com; Fax: + 49 (0) 6421 28 27016

https://doi.org/10.1021/acsami.2c02741
ACS Appl. Mater. Interfaces 2022, 14, 31525−31540

Authors

Alice Abu Dayyih − *Department of Pharmaceutics and Biopharmaceutics, University of Marburg, 35037 Marburg, Germany*

Bernd Gutberlet − *Department of Pharmaceutics and Biopharmaceutics, University of Marburg, 35037 Marburg, Germany*

Eduard Preis − *Department of Pharmaceutics and Biopharmaceutics, University of Marburg, 35037 Marburg, Germany;* orcid.org/0000-0003-2112-8436

Konrad H. Engelhardt − *Department of Pharmaceutics and Biopharmaceutics, University of Marburg, 35037 Marburg, Germany*

Muhammad Umair Amin − *Department of Pharmaceutics and Biopharmaceutics, University of Marburg, 35037 Marburg, Germany*

Ahmed M. Abdelsalam − *Department of Pharmaceutics and Biopharmaceutics, University of Marburg, 35037 Marburg, Germany; Department of Pharmaceutics and Industrial Pharmacy, Faculty of Pharmacy, Al-Azhar University, Assiut 71524, Egypt*

Martina Bonsu − *Department of Pharmaceutics and Biopharmaceutics, University of Marburg, 35037 Marburg, Germany*

Complete contact information is available at: https://pubs.acs.org/10.1021/acsami.2c02741

Author Contributions

§These authors contributed equally to this work.

Notes

The authors declare no competing financial interest.

■ ACKNOWLEDGMENTS

The authors would like to thank Mrs. Eva Mohr for her technical support in the cell culture lab and Ms. Reem Aboud for her laboratory assistance.

■ ABBREVIATIONS

AFM, atomic force microscopy
aPDT, antimicrobial photodynamic therapy
DHβCD-TSL, DiR-hypericin-2-hydroxypropyl-β cyclodextrin complex loaded thermosensitive liposomes
DiR, 1,1-dioctadecyl-3,3,3,3-tetramethylindotricarbocyanine iodide
DPPC, 1,2-dipalmitoyl-*sn*-glycero-3-phosphocholine
DRVs, dehydration-rehydration vesicles
DSC, differential scanning calorimetry
DSPC, 1,2-distearoyl-*sn*-glycero-3-phosphocholine
Hyp, hypericin
Hyp-βCD-TSL, hypericin-2-hydroxypropyl-β cyclodextrin complex loaded thermosensitive liposomes
MTT, 3-[4,5-dimethylthiazol-2-yl]-2,5-diphenyltetrazolium bromide
NIR, near-infrared
PTT, photothermal therapy
TEM, transmission electron microscopy
TSL, thermosensitive liposomes
βCD, 2-hydroxypropyl-β cyclodextrin

■ REFERENCES

(1) Reardon, S. WHO Warns against "post-Antibiotic" Era. *Nature* **2014**, DOI: 10.1038/nature.2014.15135.

(2) Renwick, M. J.; Brogan, D. M.; Mossialos, E. A Systematic Review and Critical Assessment of Incentive Strategies for Discovery and Development of Novel Antibiotics. *J. Antibiot.* **2016**, *69*, 73−88.

(3) Czaplewski, L.; Bax, R.; Clokie, M.; Dawson, M.; Fairhead, H.; Fischetti, V. A.; Foster, S.; Gilmore, B. F.; Hancock, R. E. W.; Harper, D.; Henderson, I. R.; Hilpert, K.; Jones, B. V.; Kadioglu, A.; Knowles, D.; Ólafsdóttir, S.; Payne, D.; Projan, S.; Shaunak, S.; Silverman, J.; Thomas, C. M.; Trust, T. J.; Warn, P.; Rex, J. H. Alternatives to Antibiotics—a Pipeline Portfolio Review. *Lancet Infect. Dis.* **2016**, *16*, 239−251.

(4) Wainwright, M.; Maisch, T.; Nonell, S.; Plaetzer, K.; Almeida, A.; Tegos, G. P.; Hamblin, M. R. Photoantimicrobials—Are We Afraid of the Light? *Lancet Infect. Dis.* **2017**, *17*, e49−e55.

(5) Grinholc, M.; Szramka, B.; Kurlenda, J.; Graczyk, A.; Bielawski, K. P. Bactericidal Effect of Photodynamic Inactivation against Methicillin-Resistant and Methicillin-Susceptible Staphylococcus Aureus Is Strain-Dependent. *J. Photochem. Photobiol., B* **2008**, *90*, 57−63.

(6) Fekrazad, R.; Zare, H.; Sepahvand, S. M.; Morsali, P. The Effect of Antimicrobial Photodynamic Therapy with Radachlorin® on Staphylococcus Aureus and Escherichia Coli: An in Vitro Study. *J. Lasers Med. Sci.* **2014**, *5*, 82.

(7) García, I.; Ballesta, S.; Gilaberte, Y.; Rezusta, A.; Pascual, Á. Antimicrobial Photodynamic Activity of Hypericin against Methicillin-Susceptible and Resistant Staphylococcus Aureus Biofilms. *Future Microbiol.* **2015**, *10*, 347−356.

(8) Boluki, E.; Kazemian, H.; Peeridogaheh, H.; Alikhani, M. Y.; Shahabi, S.; Beytollahi, L.; Ghorbanzadeh, R. Antimicrobial Activity of Photodynamic Therapy in Combination with Colistin against a Pan-Drug Resistant Acinetobacter Baumannii Isolated from Burn Patient. *Photodiagn. Photodyn. Ther.* **2017**, *18*, 1−5.

(9) Almeida, A.; Faustino, M. A. F.; Neves, M. G. P. M. S. Antimicrobial Photodynamic Therapy in the Control of COVID-19. *Antibiotics* **2020**, *9*, 320.

(10) Kipshidze, N.; Yeo, N.; Kipshidze, N. Photodynamic Therapy for COVID-19. *Nat. Photonics* **2020**, *14*, 651−652.

(11) Svyatchenko, V.; Nikonov, S.; Mayorov, A.; Gelfond, M.; Loktev, V. Antiviral Photodynamic Therapy: Inactivation and Inhibition of SARS-CoV-2 in Vitro Using Methylene Blue and Radachlorin. *Photodiagn. Photodyn. Ther.* **2021**, *33*, No. 102112.

(12) Plenagl, N.; Benjam, S.; Duse, L.; Pinnapireddy, S. R.; Jedelska, J.; Brüßler, J.; Bakowsky, U. Hypericin Inclusion Complexes Encapsulated in Liposomes for Antimicrobial Photodynamic Therapy. *Int. J. Pharm.* **2019**, *570*, No. 118666.

(13) Yow, C. M. N.; Tang, H. M.; Chu, E. S. M.; Huang, Z. Hypericin-Mediated Photodynamic Antimicrobial Effect on Clinically Isolated Pathogens. *Photochem. Photobiol.* **2012**, *88*, 626−632.

(14) Kleemann, B.; Loos, B.; Scriba, T. J.; Lang, D.; Davids, L. M. St John's Wort (Hypericum Perforatum L.) Photomedicine: Hypericin-Photodynamic Therapy Induces Metastatic Melanoma Cell Death. *PLoS One* **2014**, *9*, No. e103762.

(15) de Morais, F. A. P.; Gonçalves, R. S.; Vilsinski, B. H.; Lazarin-Bidóia, D.; Balbinot, R. B.; Tsubone, T. M.; Brunaldi, K.; Vatatu Nakamura, C.; Hioka, N.; Caetano, W. Hypericin Photodynamic Activity in DPPC Liposomes − Part II: Stability and Application in Melanoma B16-F10 Cancer Cells. *Photochem. Photobiol. Sci.* **2020**, 620.

(16) Plenagl, N.; Seitz, B. S.; Reddy Pinnapireddy, S.; Jedelská, J.; Brüßler, J.; Bakowsky, U. Hypericin Loaded Liposomes for Anti-Microbial Photodynamic Therapy of Gram-Positive Bacteria. *Phys. Status Solidi A* **2018**, *215*, 1700837.

(17) Lüthi, M.; Besic Gyenge, E.; Engström, M.; Bredell, M.; Grätz, K.; Walt, H.; Gmür, R.; Maake, C. Hypericin- and MTHPC-Mediated Photodynamic Therapy for the Treatment of Cariogenic Bacteria. *Med. Laser Appl.* **2009**, *24*, 227−236.

(18) Hager, B.; Strauss, W. S. L.; Falk, H. Cationic Hypericin Derivatives as Novel Agents with Photobactericidal Activity: Synthesis and Photodynamic Inactivation of Propionibacterium Acnes. *Photochem. Photobiol.* **2009**, *85*, 1201−1206.

(19) Zhang, W.; Gong, X.; Cai, Y.; Zhang, C.; Yu, X.; Fan, J.; Diao, G. Investigation of Water-Soluble Inclusion Complex of Hypericin with β-Cyclodextrin Polymer. *Carbohydr. Polym.* **2013**, *95*, 366−370.
(20) Qiu, N.; Zhao, X.; Liu, Q.; Shen, B.; Liu, J.; Li, X.; An, L. Inclusion Complex of Emodin with Hydroxypropyl-β-Cyclodextrin: Preparation, Physicochemical and Biological Properties. *J. Mol. Liq.* **2019**, *289*, No. 111151.
(21) Perni, S.; Prokopovich, P.; Pratten, J.; Parkin, I. P.; Wilson, M. Nanoparticles: Their Potential Use in Antibacterial Photodynamic Therapy. *Photochem. Photobiol. Sci.* **2011**, *10*, 712−720.
(22) Liu, M.; Du, H.; Zhang, W.; Zhai, G. Internal Stimuli-Responsive Nanocarriers for Drug Delivery: Design Strategies and Applications. *Mater. Sci. Eng., C* **2017**, *71*, 1267−1280.
(23) Dou, Y.; Hynynen, K.; Allen, C. To Heat or Not to Heat: Challenges with Clinical Translation of Thermosensitive Liposomes. *J. Controlled Release* **2017**, 63−73.
(24) Kneidl, B.; Peller, M.; Winter, G.; Lindner, L. H.; Hossann, M. Thermosensitive Liposomal Drug Delivery Systems: State of the Art Review. *Int. J. Nanomed.* **2014**, *9*, 4387−4398.
(25) Zhao, Y.; Dai, X.; Wei, X.; Yu, Y.; Chen, X.; Zhang, X.; Li, C. Near-Infrared Light-Activated Thermosensitive Liposomes as Efficient Agents for Photothermal and Antibiotic Synergistic Therapy of Bacterial Biofilm. *ACS Appl. Mater. Interfaces* **2018**, *10*, 14426−14437.
(26) Yang, Y.; Ma, L.; Cheng, C.; Deng, Y.; Huang, J.; Fan, X.; Nie, C.; Zhao, W.; Zhao, C. Nonchemotherapic and Robust Dual-Responsive Nanoagents with on-Demand Bacterial Trapping, Ablation, and Release for Efficient Wound Disinfection. *Adv. Funct. Mater.* **2018**, *28*, 1705708.
(27) Preis, E.; Anders, T.; Širc, J.; Hobzova, R.; Cocarta, A. I.; Bakowsky, U.; Jedelská, J. Biocompatible Indocyanine Green Loaded PLA Nanofibers for in Situ Antimicrobial Photodynamic Therapy. *Mater. Sci. Eng., C* **2020**, *115*, No. 111068.
(28) Sun, J.; Song, L.; Fan, Y.; Tian, L.; Luan, S.; Niu, S.; Ren, L.; Ming, W.; Zhao, J. Synergistic Photodynamic and Photothermal Antibacterial Nanocomposite Membrane Triggered by Single NIR Light Source. *ACS Appl. Mater. Interfaces* **2019**, *11*, 26581−26589.
(29) Chen, Y.; Gao, Y.; Chen, Y.; Liu, L.; Mo, A.; Peng, Q. Nanomaterials-Based Photothermal Therapy and Its Potentials in Antibacterial Treatment. *J. Controlled Release* **2020**, *328*, 251−262.
(30) Manivasagan, P.; Khan, F.; Hoang, G.; Mondal, S.; Kim, H.; Doan, V. H. M.; Kim, Y. M.; Oh, J. Thiol Chitosan-Wrapped Gold Nanoshells for near-Infrared Laser-Induced Photothermal Destruction of Antibiotic-Resistant Bacteria. *Carbohydr. Polym.* **2019**, *225*, No. 115228.
(31) Wang, J.; Guo, F.; Yu, M.; Liu, L.; Tan, F.; Yan, R.; Li, N. Rapamycin/DiR Loaded Lipid-Polyaniline Nanoparticles for Dual-Modal Imaging Guided Enhanced Photothermal and Antiangiogenic Combination Therapy. *J. Controlled Release* **2016**, *237*, 23−34.
(32) Youniss, F. M.; Sundaresan, G.; Graham, L. J.; Wang, L.; Berry, C. R.; Dewkar, G. K.; Jose, P.; Bear, H. D.; Zweit, J. Near-Infrared Imaging of Adoptive Immune Cell Therapy in Breast Cancer Model Using Cell Membrane Labeling. *PLoS One* **2014**, *9*, No. e109162.
(33) He, X.; Bao, X.; Cao, H.; Zhang, Z.; Yin, Q.; Gu, W.; Chen, L.; Yu, H.; Li, Y. Tumor-Penetrating Nanotherapeutics Loading a near-Infrared Probe Inhibit Growth and Metastasis of Breast Cancer. *Adv. Funct. Mater.* **2015**, *25*, 2831−2839.
(34) Liu, H.; Wu, D. In Vivo Near-Infrared Fluorescence Tumor Imaging Using DiR-Loaded Nanocarriers. *Curr. Drug Delivery* **2016**, *13*, 40−48.
(35) Raschpichler, M.; Agel, M. R.; Pinnapireddy, S. R.; Duse, L.; Baghdan, E.; Schäfer, J.; Bakowsky, U. *In Situ* Intravenous Photodynamic Therapy for the Systemic Eradication of Blood Stream Infections. *Photochem. Photobiol. Sci.* **2019**, *18*, 304−308.
(36) Angelini, G.; Campestre, C.; Boncompagni, S.; Gasbarri, C. Liposomes Entrapping β-Cyclodextrin/Ibuprofen Inclusion Complex: Role of the Host and the Guest on the Bilayer Integrity and Microviscosity. *Chem. Phys. Lipids* **2017**, *209*, 61−65.
(37) Higuchi, T.; Connors, K. A. In *Advances in Analytical Chemistry and Instrumentation*; Phase Solubility Techniques. 1965.
(38) Pîrnau, A.; Bogdan, M.; Floare, C. G. NMR Spectroscopic Characterization of β-Cyclodextrin Inclusion Complex with Vanillin. *J. Phys.: Conf. Ser.* **2009**, *182*, No. 012013.
(39) Brüßler, J.; Strehlow, B.; Becker, A.; Schubert, R.; Schümmelfeder, J.; Nimsky, C.; Bakowsky, U. Nanoscaled Ultrasound Contrast Agents for Enhanced Sonothrombolysis. *Colloids Surf., B* **2018**, *172*, 728−733.
(40) Engelhardt, K. H.; Pinnapireddy, S. R.; Baghdan, E.; Jedelská, J.; Bakowsky, U. Transfection Studies with Colloidal Systems Containing Highly Purified Bipolar Tetraether Lipids from Sulfolobus Acidocaldarius. *Archaea* **2017**, *2017*, No. 8047149.
(41) Entradas, T.; Waldron, S.; Volk, M. The Detection Sensitivity of Commonly Used Singlet Oxygen Probes in Aqueous Environments. *J. Photochem. Photobiol. B* **2020**, *204*, No. 111787.
(42) Ayoub, A. M.; Amin, M. U.; Ambreen, G.; Dayyih, A. A.; Abdelsalam, A. M.; Somaida, A.; Engelhardt, K.; Wojcik, M.; Schäfer, J.; Bakowsky, U. Photodynamic and Antiangiogenic Activities of Parietin Liposomes in Triple Negative Breast Cancer. *Mater. Sci. Eng., C* **2021**, *October*, No. 112543.
(43) Jun, G.; Yong, Z.; Jinghao, P. The Determination of β-Cyclodextrin by Ultraviolet Spectrophotometry. *Microchem. J.* **1998**, *60*, 26−31.
(44) Vögeling, H.; Plenagl, N.; Seitz, B. S.; Pinnapireddy, S. R.; Dayyoub, E.; Jedelska, J.; Brüßler, J.; Bakowsky, U. Synergistic Effects of Ultrasound and Photodynamic Therapy Leading to Biofilm Eradication on Polyurethane Catheter Surfaces Modified with Hypericin Nanoformulations. *Mater. Sci. Eng., C* **2019**, *103*, No. 109749.
(45) Plenagl, N.; Duse, L.; Seitz, B. S.; Goergen, N.; Pinnapireddy, S. R.; Jedelska, J.; Brüßler, J.; Bakowsky, U. Photodynamic Therapy − Hypericin Tetraether Liposome Conjugates and Their Antitumor and Antiangiogenic Activity. *Drug Delivery* **2019**, *26*, 23−33.
(46) Noreña-Caro, D.; Alvarez-Láinez, M. Experimental Design as a Tool for the Manufacturing of Filtering Media Based on Electrospun Polyacrylonitrile/ β -Cyclodextrin Fibers. *Int. J. Interact. Des. Manuf.* **2016**, *10*, 153−164.
(47) Pôrnău, A.; Mic, M.; Bogdan, M.; Turcu, I. Characterization of β-Cyclodextrin Inclusion Complex with Procaine Hydrochloride by 1H NMR and ITC. *J. Inclusion Phenom. Macrocyclic Chem.* **2014**, *79*, 283−289.
(48) Tatsis, E. C.; Exarchou, V.; Troganis, A. N.; Gerothanassis, I. P. 1H NMR Determination of Hypericin and Pseudohypericin in Complex Natural Mixtures by the Use of Strongly Deshielded OH Groups. *Anal. Chim. Acta* **2008**, *607*, 219−226.
(49) Zhang, W.; Chen, M.; Diao, G. Preparation and Electrochemical Behavior of Water-Soluble Inclusion Complex of Ferrocene with β-Cyclodextrin Polymer. *Electrochim. Acta* **2011**, *56*, 5129−5136.
(50) Barras, A.; Boussekey, L.; Courtade, E.; Boukherroub, R. Hypericin-Loaded Lipid Nanocapsules for Photodynamic Cancer Therapy in Vitro. *Nanoscale* **2013**, *5*, 10562−10572.
(51) Spikes, J. D. Quantum Yields and Kinetics of the Photobleaching of Hematoporphyrin, Porphine and Uroporphyrin Photofrin 11, Tetra(4-Sulfonat0phenyl) Porphine and Uroporphyrin. *Photochem. Photobiol.* **1992**, *55*, 797−808.
(52) Ayoub, A. M.; Gutberlet, B.; Preis, E.; Abdelsalam, A. M.; Abu Dayyih, A.; Abdelkader, A.; Balash, A.; Schäfer, J.; Bakowsky, U. Parietin Cyclodextrin-Inclusion Complex as an Effective Formulation for Bacterial Photoinactivation. *Pharmaceutics* **2022**, *14*, 357.
(53) Saw, C. L. L.; Olivo, M.; Soo, K. C.; Heng, P. W. S. Spectroscopic Characterization and Photobleaching Kinetics of Hypericin-N-Methyl Pyrrolidone Formulations. *Photochem. Photobiol. Sci.* **2006**, *5*, 1018−1023.
(54) Klausen, M.; Ucuncu, M.; Bradley, M. Design of Photosensitizing Agents for Targeted Antimicrobial Photodynamic Therapy. *Molecules* **2020**, *25*, 5239.
(55) Ioele, G.; De Luca, M.; Garofalo, A.; Ragno, G. Photosensitive Drugs: A Review on Their Photoprotection by Liposomes and Cyclodextrins. *Drug Delivery* **2017**, *24*, 33−44.

(56) Hurler, J.; Žakelj, S.; Mravljak, J.; Pajk, S.; Kristl, A.; Schubert, R.; Škalko-Basnet, N. The Effect of Lipid Composition and Liposome Size on the Release Properties of Liposomes-in-Hydrogel. *Int. J. Pharm.* **2013**, *456*, 49−57.
(57) Akimoto, J.; Nakayama, M.; Okano, T. Temperature-Responsive Polymeric Micelles for Optimizing Drug Targeting to Solid Tumors. *J. Controlled Release* **2014**, *193*, 2−8.
(58) Abu Dayyih, A.; Alawak, M.; Ayoub, A. M.; Amin, M. U.; Abu Dayyih, W.; Engelhardt, K.; Duse, L.; Preis, E.; Brüßler, J.; Bakowsky, U. Thermosensitive Liposomes Encapsulating Hypericin: Characterization and Photodynamic Efficiency. *Int. J. Pharm.* **2021**, *609*, No. 121195.
(59) Qing, G.; Zhao, X.; Gong, N.; Chen, J.; Li, X.; Gan, Y.; Wang, Y.; Zhang, Z.; Zhang, Y.; Guo, W.; Luo, Y.; Liang, X.-J. Thermo-Responsive Triple-Function Nanotransporter for Efficient Chemo-Photothermal Therapy of Multidrug-Resistant Bacterial Infection. *Nat. Commun.* **2019**, *10*, 1−12.
(60) Wang, W.; Cheng, X.; Liao, J.; Lin, Z.; Chen, L.; Liu, D.; Zhang, T.; Li, L.; Lu, Y.; Xia, H. Synergistic Photothermal and Photodynamic Therapy for Effective Implant-Related Bacterial Infection Elimination and Biofilm Disruption Using Cu9S8 Nanoparticles. *ACS Biomater. Sci. Eng.* **2019**, *5*, 6243−6253.
(61) Li, H.; Zhou, X.; Huang, Y.; Liao, B.; Cheng, L.; Ren, B. Reactive Oxygen Species in Pathogen Clearance: The Killing Mechanisms, the Adaption Response, and the Side Effects. *Front. Microbiol.* **2021**, *11*, No. 622534.
(62) Dai, Y.; Du, W.; Gao, D.; Zhu, H.; Zhang, F.; Chen, K.; Ni, H.; Li, M.; Fan, Q.; Shen, Q. Near-Infrared-II Light Excitation Thermosensitive Liposomes for Photoacoustic Imaging-Guided Enhanced Photothermal-Chemo Synergistic Tumor Therapy. *Biomater. Sci.* **2022**, *10*, 435−443.
(63) Allison, R. R.; Downie, G. H.; Cuenca, R.; Hu, X. H.; Childs, C. J. H.; Sibata, C. H. Photosensitizers in Clinical PDT. *Photodiagn. Photodyn. Ther.* **2004**, *1*, 27−42.
(64) Henderson, B. W.; Busch, T. M.; Snyder, J. W. Fluence Rate as a Modulator of PDT Mechanisms. *Lasers Surg. Med.* **2006**, *38*, 489−493.
(65) Maldonado-Carmona, N.; Ouk, T. S.; Calvete, M. J. F.; Pereira, M. M.; Villandier, N.; Leroy-Lhez, S. Conjugating Biomaterials with Photosensitizers: Advances and Perspectives for Photodynamic Antimicrobial Chemotherapy. *Photochem. Photobiol. Sci.* **2020**, *19*, 445−461.
(66) Hegge, A. B.; Vukicevic, M.; Bruzell, E.; Kristensen, S.; Tønnesen, H. H. Solid Dispersions for Preparation of Phototoxic Supersaturated Solutions for Antimicrobial Photodynamic Therapy (APDT): Studies on Curcumin and Curcuminoides L. *Eur. J. Pharm. Biopharm.* **2013**, *83*, 95−105.
(67) Ribeiro, C. P. S.; Gamelas, S. R. D.; Faustino, M. A. F.; Gomes, A. T. P. C.; Tomé, J. P. C.; Almeida, A.; Lourenço, L. M. O. Unsymmetrical Cationic Porphyrin-Cyclodextrin Bioconjugates for Photoinactivation of Escherichia Coli. *Photodiagn. Photodyn. Ther.* **2020**, *31*, No. 101788.
(68) Mora, S. J.; Cormick, M. P.; Milanesio, M. E.; Durantini, E. N. The Photodynamic Activity of a Novel Porphyrin Derivative Bearing a Fluconazole Structure in Different Media and against Candida Albicans. *Dyes Pigm.* **2010**, *87*, 234−240.
(69) Gao, Y.; Wang, J.; Hu, D.; Deng, Y.; Chen, T.; Jin, Q.; Ji, J.; Gao, Y. F.; Wang, J.; Hu, D. F.; Deng, Y. Y.; Chen, T. T.; Jin, Q.; Ji, J. Bacteria-Targeted Supramolecular Photosensitizer Delivery Vehicles for Photodynamic Ablation against Biofilms. *Macromol. Rapid Commun.* **2019**, *40*, 1800763.
(70) Polat, E.; Kang, K. Natural Photosensitizers in Antimicrobial Photodynamic Therapy. *Biomedicines* **2021**, *9*, 584.
(71) Zhang, J.; Zhang, F.; Tang, Q.; Xu, C.; Meng, X. Effect of Photodynamic Inactivation of Escherichia Coli by Hypericin. *World J. Microbiol. Biotechnol.* **2018**, *34*, 100.
(72) Paz-Cristobal, M. P.; Royo, D.; Rezusta, A.; Andrés-Ciriano, E.; Alejandre, M. C.; Meis, J. F.; Revillo, M. J.; Aspiroz, C.; Nonell, S.; Gilaberte, Y. Photodynamic Fungicidal Efficacy of Hypericin and Dimethyl Methylene Blue against Azole-Resistant Candida Albicans Strains. *Mycoses* **2014**, *57*, 35−42.
(73) Monjo, A.; Pringle, E.; Thornbury, M.; Duguay, B.; Monro, S.; Hetu, M.; Knight, D.; Cameron, C.; McFarland, S.; McCormick, C. Photodynamic Inactivation of Herpes Simplex Viruses. *Viruses* **2018**, *10*, 532.
(74) Tawakoli, P. N.; Al-Ahmad, A.; Hoth-Hannig, W.; Hannig, M.; Hannig, C. Comparison of Different Live/Dead Stainings for Detection and Quantification of Adherent Microorganisms in the Initial Oral Biofilm. *Clin Oral Investig.* **2013**, *17*, 841−850.
(75) Baghdan, E.; Raschpichler, M.; Lutfi, W.; Pinnapireddy, S. R.; Pourasghar, M.; Schäfer, J.; Schneider, M.; Bakowsky, U. Nano Spray Dried Antibacterial Coatings for Dental Implants. *Eur. J. Pharm. Biopharm.* **2019**, *139*, 59−67.
(76) Li, P.; Song, J.; Ni, X.; Guo, Q.; Wen, H.; Zhou, Q.; Shen, Y.; Huang, Y.; Qiu, P.; Lin, S.; Hu, H. Comparison in Toxicity and Solubilizing Capacity of Hydroxypropyl-β-Cyclodextrin with Different Degree of Substitution. *Int. J. Pharm.* **2016**, *513*, 347−356.
(77) Gould, S.; Scott, R. C. 2-Hydroxypropyl-β-Cyclodextrin (HP-β-CD): A Toxicology Review. *Food Chem. Toxicol.* **2005**, *43*, 1451−1459.

https://doi.org/10.1021/acsami.2c02741
ACS Appl. Mater. Interfaces 2022, 14, 31525−31540